bioRxiv preprint doi: https://doi.org/10.1101/2021.03.18.436026; this version posted March 18, 2021. The copyright holder for this preprint (which was not certified by peer review) is the author/funder, who has granted bioRxiv a license to display the preprint in perpetuity. It is made available under aCC-BY 4.0 International license.

Full title: Infection of immune competent macrophages expressing functional Slc11a1 alters global gene expression, regulation of metal ions, and infection outcomes

Short title: Slc11a1 alters nutritional immunity

Lara N. Janiszewski[1], Michael Minson[1], Mary A. Allen[2], Robin D. Dowell[2], Amy E Palmer[1, *]

Author affiliations

1 Department of Biochemistry and BioFrontiers Institute, University of Colorado Boulder, Boulder CO 80303

2 Department of Molecular Cellular Developmental Biology and BioFrontiers Institute, University of Colorado Boulder, Boulder CO 80303

* To whom correspondence should be addressed: amy.palmer@colorado.edu

Keywords: metal, zinc, macrophages, Salmonella, Slc11a1, RNAseq, nutritional immunity

bioRxiv preprint doi: https://doi.org/10.1101/2021.03.18.436026; this version posted March 18, 2021. The copyright holder for this preprint (which was not certified by peer review) is the author/funder, who has granted bioRxiv a license to display the preprint in perpetuity. It is made available under aCC-BY 4.0 International license.

Abstract:

Nutritional immunity involves cellular and physiological responses to invading pathogens, such as limiting iron availability, increasing exposure to bactericidal copper, and manipulating zinc to restrict the growth of pathogens. Manipulation of zinc at the host-pathogen interface depends on both the pathogen's identity and the nature of the host cell. Here we examine infection of bone marrow-derived macrophages from 129S6/SvEvTac mice by *Salmonella* Typhimurium. Unlike Balb/c and C57BL/6 mice, 129S6/SvEvTac mice possess a functional Slc11a1 (Nramp-1), a phagosomal transporter of divalent cations. We carried out global RNA sequencing upon treatment with live or heat-killed *Salmonella* at 2 Hrs and 18 Hrs post-infection and observed widespread changes in metal transport, metal-dependent, and metal homeostasis genes, suggesting significant remodeling of iron, copper, and zinc availability by host cells. Changes in host cell gene expression suggest infection increases cytosolic zinc while simultaneously limiting zinc within the phagosome. Using a genetically encoded sensor, we demonstrate that cytosolic labile zinc increases 36-fold 12 hrs post-infection. Further, manipulation of zinc in the media alters bacterial clearance and replication, with zinc depletion inhibiting both processes. Comparing our results to published data on infection of C57BL/6 macrophages revealed notable differences in metal regulation and the global immune response, with 129S6 macrophages transitioning from M1 to M2 polarization over the course of infection and showing signs of recovery. Our results reveal that functional Slc11a1 profoundly affects the transcriptional landscape upon infection. Further, our results indicate that manipulation of zinc at the host-pathogen interface is more nuanced than that of iron or copper. 129S6 macrophage leverage intricate means of manipulating zinc availability and

bioRxiv preprint doi: https://doi.org/10.1101/2021.03.18.436026; this version posted March 18, 2021. The copyright holder for this preprint (which was not certified by peer review) is the author/funder, who has granted bioRxiv a license to display the preprint in perpetuity. It is made available under aCC-BY 4.0 International license.

distribution to limit the pathogen's access to zinc while simultaneously ensuring sufficient zinc to support the immune response.

Author summary: Metal ions play an important role in influencing how immune cells such as macrophages respond to infection by pathogens. Because metal ions are both essential to survival, as well toxic when present is excessive amounts, the host and the pathogen have evolved diverse strategies to regulate metal acquisition and availability. Here, we show that the metal transporter slc11a1 plays a critical role in defining the host response to Salmonella infection. Infection causes widespread changes in expression of metal regulatory genes to limit the pathogen's access to iron, increase its exposure to copper, and remodel zinc to ensure increased zinc in the cytosol and limited zinc for the pathogen. Macrophages expressing functional slc11a1 have a different profile of metal regulation and vastly different outcomes compared to immune compromised macrophage, demonstrating significantly different nutritional immune responses in immune competent versus immune compromised macrophages.

bioRxiv preprint doi: https://doi.org/10.1101/2021.03.18.436026; this version posted March 18, 2021. The copyright holder for this preprint (which was not certified by peer review) is the author/funder, who has granted bioRxiv a license to display the preprint in perpetuity. It is made available under aCC-BY 4.0 International license.

Introduction

Pathogenic organisms must acquire essential micronutrients such as iron, zinc, and manganese to sustain growth and maintain pathogenicity. To protect itself, a host organism in turn attempts to sequester these nutrients, as unfettered access can allow for the exponential growth of an invasive microbe population(1). Metal ion sequestration occurs on a systemic level, evidenced by the sharp decrease of free metal ions in serum upon infection(2). Additionally, phagocytic immune cells manipulate the intracellular localization of metal ions to limit the viability of engulfed pathogens, but this process is more complex than unilateral sequestration. Within macrophages, iron (Fe) ions are bound by cytosolic storage proteins and transported out of phagosomal compartments(3), while these same compartments are flooded with bactericidal copper (Cu) ions(4,5). The role of zinc (Zn) in nutritional immunity in macrophages is more nuanced than that of Fe or Cu, as it can be used either to poison or starve a pathogen(1). Some microbes have developed strategies to counter these tactics, including siderophores to scavenge Fe ions, oxidases to detoxify Cu, exporters to expunge excess metals, and high-affinity importers to overcome metal limitation(1,2,6). There is a growing body of work suggesting that both the pathogen and the host have mechanisms to regulate Zn accessibility(1,7), however the overall picture of Zn regulation during infection is not well understood.

Zn is an essential micronutrient required for growth, proliferation, and several fundamental biological processes. In mammals, Zn is a requisite cofactor either structurally or catalytically for approximately 10% of the proteome(8), including many transcription factors and enzymes. As with other metal ions, excess Zn can be toxic, and cells tightly regulate its

bioRxiv preprint doi: https://doi.org/10.1101/2021.03.18.436026; this version posted March 18, 2021. The copyright holder for this preprint (which was not certified by peer review) is the author/funder, who has granted bioRxiv a license to display the preprint in perpetuity. It is made available under aCC-BY 4.0 International license.

availability. Mammalian cells contain hundreds of micromolar total Zn but most of this is bound to proteins, enzymes and other ligands such that labile (or exchangeable) Zn, as measured by fluorescent sensors, is typically in the hundreds of picomolar range in the cytosol(9–11). There are fewer tools for, and hence less consensus on, the concentration of labile Zn in organelles. However, multiple different fluorescent sensor platforms have suggested that labile Zn distribution in organelles is heterogeneous(11–15). Zn is regulated by membrane-specific Zn transporters, including Slc30a1-10 (also referred to as ZnT1-10) that transport zinc out of the cytosol, and Slc39a1-14 (also referred to as Zip1-14) that transport Zn (as well as Fe and manganese, Mn) into the cytosol(16). Cells also contain metallothioneins (Mt), which serve to bind and buffer Zn ions, and a metal-dependent transcription factor (Mtf1) that translocates to the nucleus upon binding excess Zn to regulate the expression of genes that lower cytosolic Zn levels. One major role of Mtf1 is regulating the expression of Mt genes in response to cytosolic Zn levels, protecting cells from fluctuations in environmental Zn(17). Consequently, increased Mt expression is often used as a proxy for increased cytosolic Zn.

How macrophages use Zn to fight infection seems to depend on the pathogen it encounters, as well as the nature of the host cell. Macrophages poison *M. tb, S. pneumoniae, E. coli, and H. pylori* by transporting toxic levels of Zn into pathogen-containing phagosomes(18–21). Conversely, challenge with *Histoplasma capsulatum* induces macrophages to sequester Zn and increase ROS production to counter the infection(22). There does not appear to be consensus regarding Zn manipulation upon infection with *Salmonella* Typhimurium. *Salmonella* possess genes that aid in surviving Zn toxicity and starvation(23–26), and studies done in different types of macrophage have suggested that Zn can both facilitate and impair infection.

bioRxiv preprint doi: https://doi.org/10.1101/2021.03.18.436026; this version posted March 18, 2021. The copyright holder for this preprint (which was not certified by peer review) is the author/funder, who has granted bioRxiv a license to display the preprint in perpetuity. It is made available under aCC-BY 4.0 International license.

In a study of macrophages derived from primary human monocytes and the human monocyte THP-1 cell line, infection induces Zn to accumulate in punctate vesicular compartments, though *Salmonella* managed to avoid these toxic Zn compartments via an SPI-1-dependent mechanism(27). In contrast, *Salmonella* infection of the mouse RAW264.7 macrophage cell line induced Zn mobilization, and increased Zn correlated with impaired bacterial clearance(26). On the other hand, multiple studies have revealed that the high-affinity ZnuABC zinc uptake system and associated accessory proteins are critical virulence factors in *Salmonella*, suggesting that *Salmonella* experience Zn starvation inside the host(23,24,28). Critical comparison of Zn at the host-pathogen interface may be confounded by the differences in the macrophage models used across studies. For example, both Balb/c and C57BL/6 mice lack a functional Slc11a1 (Nramp-1), a phagosomal transporter for magnesium (Mg), Fe, Mn, and Zn(29). Macrophages from these mice are more susceptible to infection and have a reduced capacity to clear intracellular pathogens(30). RAW264.7 cells, a popular mouse macrophage cell line used to study intracellular pathogens, are derived from C57BL/6 mice and therefore equally impaired. The lack of functional Slc11a1 is also likely to compromise the host response to infection with respect to metal regulation, making it difficult to define the nutritional immunity landscape in an immune-competent model system.

In this study, we carried out global RNA sequencing upon infection of macrophages from 129S6 mice with *Salmonella* Typhimurium and examined the changes in gene expression via clustering, and gene set enrichment analysis (GSEA). We deliberately used the 129S6/SvEvTac (hereafter referred to as 129S6) mouse because it contains a functional Slc11a1 protein and has been used as a model system for chronic systemic infection(30). We examined changes in

bioRxiv preprint doi: https://doi.org/10.1101/2021.03.18.436026; this version posted March 18, 2021. The copyright holder for this preprint (which was not certified by peer review) is the author/funder, who has granted bioRxiv a license to display the preprint in perpetuity. It is made available under aCC-BY 4.0 International license.

metal-regulatory and metal-dependent genes and compared our results to published data on infection of C57BL/6 mice. While some changes in metal regulatory genes were similar between the two different model systems, suggesting common mechanisms of altering metals at the host-pathogen interface, there were also notable differences, indicating that functional Slc11a1 does alter the nutritional immunity landscape within the host. We also found that cytosolic Zn levels increased over the course of infection and that Zn availability alters infection outcome. Specifically, we found that Zn supports increased replication of intracellular bacteria, but also facilitates clearance of bacteria from macrophages. Our results indicate that functional Slc11a1 significantly affects changes in gene expression, including the immune response, metal regulation in response to infection, and infection outcomes.

Results

Infection induces widespread changes in gene expression

To study metal homeostasis during infection, we used bone marrow derived macrophages (BMDMs) from 129S6 mice containing functional Slc11a1. Slc11a1 plays a critical role in regulating metal homeostasis and is important for allowing macrophages to mount an effective immune response to bacterial pathogens(29,30). To distinguish changes in macrophage gene expression in response to *Salmonella* infection from gene expression changes due to bacterial exposure, macrophages were treated with live or heat-killed *Salmonella enterica* serovar Typhimurium (hereafter referred to as *Salmonella*). Macrophages that were subjected to media changes but not exposed to *Salmonella* served as a control. To examine both early and late immune responses, macrophages were lysed at 2 or 18 hours post bacterial

bioRxiv preprint doi: https://doi.org/10.1101/2021.03.18.436026; this version posted March 18, 2021. The copyright holder for this preprint (which was not certified by peer review) is the author/funder, who has granted bioRxiv a license to display the preprint in perpetuity. It is made available under aCC-BY 4.0 International license.

exposure and subjected to global RNA sequencing (**Fig 1A**). Principal component analysis shows that samples clustered predominantly by time post infection and status of bacteria (alive versus heat killed, **Fig 1B**).

We identified 7766 genes that were differentially expressed and performed hierarchical clustering to examine the main patterns of gene expression changes. We limited analysis to genes with significant differential expression (adjusted p-value (padj) < 0.01), as determined by a DESeq2 log ratio test. An expression level cutoff was also applied (see Methods). An unsupervised algorithm (degPatterns function in DEGreport R package) was used to cluster genes based on similar expression profiles across all conditions. Twenty groups, each with at least 15 genes, emerged. Some groups showed time dependent expression, with little change between bacterial conditions, while others showed significant differences in expression upon treatment with alive versus heat-killed bacteria. Additionally, some groups were different based primarily on expression levels in control cells.

In **Fig 2** we highlight the four different expression patterns that encompass the largest gene groups. The remaining groups are presented in **Supplementary Fig S1, S2, S3, and S4** and the genes associated with each group are presented in **Supplementary Dataset 1**. We used DAVID Bioinformatics Resources 6.8 to annotate molecular functions and biological processes associated with the different gene expression clusters. **Fig 2A** presents group 1, which consists of genes with time-dependent increases in expression. These genes respond to the presence of *Salmonella* regardless of its live or heat-killed (HK) status, and are enriched for mitochondrial function (e.g. oxidative phosphorylation, ATP production), ER-Golgi transport and protein folding, immune response, sugar metabolism, and protein degradation (including proteasome

bioRxiv preprint doi: https://doi.org/10.1101/2021.03.18.436026; this version posted March 18, 2021. The copyright holder for this preprint (which was not certified by peer review) is the author/funder, who has granted bioRxiv a license to display the preprint in perpetuity. It is made available under aCC-BY 4.0 International license.

and unfolded protein response genes). Specific genes that are characteristic of the M2 anti-inflammatory immune response(31) such as *il4rα*, *arg1*, *timp1,* and *fcgr2b* are present in this group, along with master regulators of the lipopolysaccharide (LPS) immune response *ifit1*, *stat2*, and *irf7*. Finally, genes involved in pH and redox homeostasis such as *sod1*, *nos2*, *hif1α*, carbonic anhydrases *car2/4/13*, as well as metal regulatory *slc11a1*, iron sequestering *lcn2*, and ferritin iron storage *fth1* are found in this group. Finally, *s100a8*, a metal-binding protein that is a component of calprotectin and plays a prominent role in nutritional immunity exhibited a similar expression pattern, with low expression at 2 Hrs and a significant increase at 18 Hrs (**Supplementary Fig S1D**). These results indicate that the M2 anti-inflammatory response along with many metal associated genes are upregulated over time in response to infection, regardless of whether the bacteria are alive or HK.

The genes in group 2 (**Fig 2B**) are upregulated at 2 Hrs, with higher expression in alive compared to HK conditions, and are subsequently suppressed below baseline at 18 Hrs. This group is enriched in proinflammatory M1 immune genes(31), including *tnf*, the inflammasome component *nlrp3*, and *irf1* responsible for activating cytokine production. This group also contains multiple genes involved in membrane transport of zinc (*slc30a4*, *slc39a6/a8/a10*). Another hallmark proinflammatory M1 marker *tlr2* and metal regulatory genes (the zinc-dependent transcription factor *mtf1* and iron storage ferritin light chain *ftl1*) are present in group 3 (**Supplementary Fig S1A**, which is similar to group 2 across time but differs in alive vs HK expression at 2 Hrs. Combined, these two groups indicate that in macrophages with functional *slc11a1*, much of the pro-inflammatory response is activated at early time points and then suppressed later in infection.

bioRxiv preprint doi: https://doi.org/10.1101/2021.03.18.436026; this version posted March 18, 2021. The copyright holder for this preprint (which was not certified by peer review) is the author/funder, who has granted bioRxiv a license to display the preprint in perpetuity. It is made available under aCC-BY 4.0 International license.

Fig 2C (group 8) shows genes expressed in the absence of bacterial exposure and distinctly downregulated upon infection over time. This group is notable for its relatively small number of GO annotations, which are focused on cell cycle, cell motility, zinc-binding and transport, and transcription. Noteworthy genes in group 8 include cytosolic zinc exporters *slc30a1/a5* and iron exporter *slc40a1*. Finally, **Fig 2D** demonstrates group 10 in which genes are suppressed at 2 Hrs post-infection and upregulated above untreated cells at 18 Hrs. This group is enriched for metabolism, protein export, and transcription. Specifically, these genes are involved in ER and Golgi trafficking, respiration, lysosomal activity, zinc transport (*slc39a3/a7*), iron-dependent functions (cytochrome bs, glutaredoxin2, NADH dehydrogenase), mRNA and phospholipid transport, and autophagy. Approximately 10% of these genes are involved in transcription, and half of these transcription factors bind zinc. Also in this cluster are key inflammation-related genes *tlr4* which binds lipopolysaccharide (LPS) and *irf2/3/10* which mediate the Type I IFN response. Combined, these gene expression patterns reveal remodeling of metal homeostasis, metabolism and transcription during infection.

GSEA reveals pathways differentially affected by live versus heat-killed bacteria

In analyzing global transcription patterns, we found that some groups contain differences in gene expression between live and heat killed bacterial treatments (see groups 4, 5, 7 and 16 as examples), revealing genes that respond differently to a generalized LPS trigger (HK bacteria) vs *Salmonella* with active virulence mechanisms. To identify biological processes or signaling pathways underlying these differences, GSEA(32) was performed on differentially expressed ranked gene list from Alive vs HK at 2 hours, and Alive vs HK at 18 hours. Several

bioRxiv preprint doi: https://doi.org/10.1101/2021.03.18.436026; this version posted March 18, 2021. The copyright holder for this preprint (which was not certified by peer review) is the author/funder, who has granted bioRxiv a license to display the preprint in perpetuity. It is made available under aCC-BY 4.0 International license.

significant gene sets were enriched in macrophages treated with live versus HK *Salmonella*, as defined by a false discovery rate of $q < 0.05$. When using the Hallmark Gene Set from the Molecular Signatures Database(33), we found 47 gene sets enriched at 2 Hrs, and 14 gene sets enriched at 18 Hrs for live versus HK treatment (**Supplementary Dataset S2**). One gene set that is significantly enriched in live *Salmonella* vs HK exposure at both time points is hypoxia **(Fig 3A, 3B)**. Hypoxia is an important aspect of the *in vivo* immune response to infection as hypoxia accompanies inflammation, and a hypoxic environment may affect macrophage M1/M2 polarization(31,34). Hypoxia is also accompanied by decreased glucose, increased lactate, and decreased pH, and as discussed above, we observed an increase in *hif1α*, carbonic anhydrases, and *nos2*. Multiple studies have shown activation of hypoxia induced factors upon infection of macrophages, and hypoxia is generally associated with macrophage stress as well as defense against bacterial replication(34–36). However, prolonged hypoxia is associated with tissue damage, so the severity and duration of hypoxia is an important factor in infection.

The complement gene set is activated more strongly in macrophages infected with live *Salmonella*. The complement system is part of the innate immune response and mediates a host responses such as opsonization, inflammation and direct bacterial lysis(37). Complement systems respond to bacterial coat components(38) and were therefore expected to respond similarly to live and HK *Salmonella*. Instead, many of these genes showed upregulation in live vs HK conditions **(Fig 3C, 3D)**. At two Hrs post infection, the complement leading edge is enriched for zymogens, enzymes, and secreted proteins, while at 18 Hrs there are more chemokine- and Fc-signaling related genes. At both timepoints, live conditions show upregulation of matrix metalloproteinases *mmp12* and *mmp13* and their inhibitor *timp1*. Additionally, this gene set

bioRxiv preprint doi: https://doi.org/10.1101/2021.03.18.436026; this version posted March 18, 2021. The copyright holder for this preprint (which was not certified by peer review) is the author/funder, who has granted bioRxiv a license to display the preprint in perpetuity. It is made available under aCC-BY 4.0 International license.

229 includes members of the coagulation pathway (*plaur*, *serpin*, *f3*) which overlaps and interacts
230 with complement to trap and kill microbes. Bacteria co-evolved with the complement system,
231 and many bacteria, including *Salmonella*, possess arsenals of anti-complement proteins.
232 Frequently anti-complement proteins work directly against host proteins, but our data suggest
233 live *Salmonella* affect complement gene transcription.

234 TNFα signaling via NF-κB is also more strongly activated by live *Salmonella*. During
235 infection multiple signaling cascades activate the transcription factor NF-κB, including the
236 proinflammatory cytokine TNFα (TNF in mice). NF-κB is a master regulator and specifically
237 responds to TNF activation with pro-inflammatory and anti-apoptotic signaling. At both 2 Hrs
238 and 18 Hrs, live infected samples were enriched for pro-inflammatory genes, while each time
239 point was enriched in a different set of anti-apoptotic genes **(Supplementary Fig S5)**. At two Hrs
240 *btg2*, *egr3*, *jun*, *vegfa*, *klf4* and *nr4a* were enriched in alive conditions compared to HK, while at
241 18 Hrs *bcl6*, *smad3*, *stat5a*, *plaur* and *socs3* were upregulated in alive versus HK. Most genes
242 present in the leading edge for both time points were more highly expressed at 2 Hrs,
243 reinforcing the trend of macrophages moving toward an M2-like state later in infection.

244 We also observed gene sets that were enriched only at 2 Hrs or 18 Hrs. For example, the
245 Hallmark Apoptosis gene set was enriched at 2 hours, and Hallmark Unfolded Protein Response
246 (UPR) was enriched at 18 hours **(Fig 4)**. Late log phase growth induces maximal expression of
247 *Salmonella* Pathogenicity Island 1 (SPI1) genes which allow *Salmonella* to be highly invasive and
248 frequently induce apoptosis in macrophages(39). To promote longer term infections, the
249 *Salmonella* in this experiment were grown to stationary phase before infection, which reduces
250 their expression of SPI1 genes. However, several pro-apoptosis genes are upregulated in Alive

bioRxiv preprint doi: https://doi.org/10.1101/2021.03.18.436026; this version posted March 18, 2021. The copyright holder for this preprint (which was not certified by peer review) is the author/funder, who has granted bioRxiv a license to display the preprint in perpetuity. It is made available under aCC-BY 4.0 International license.

exposure at 2 Hrs including the cAMP-dependent transcription factor *atf3*, *jun*, and *pmaip1*. The fact that the apoptotic pathway is not enriched at 18 Hrs suggests that the macrophages manage this response. While UPR and apoptosis are both possible responses to metabolic and ER stress, the upregulation of UPR at 18 Hrs could represent an attempt to restore cellular homeostasis. The transition from apoptosis genes at 2 Hrs to UPR genes at 18 Hrs correlates with a shift in macrophage polarization and may imply decreased ER stress over time.

There is significant remodeling of metal homeostasis in response to infection

One of our primary goals in carrying out RNAseq upon infection of 129S6 BMDMs was to define infection-related changes in transition metal regulatory and dependent genes in a model system with functional Slc11a1 (NRAMP1). This allows us to inform our understanding of nutritional immunity in an immune competent model system. **Fig 5A** shows several major metal regulatory proteins in macrophages. This includes Slc39a1-14 (Zip) transporters that facilitate entry of Zn, as well as Mn and Fe for some Slc39a members, into the cytosol, Slc30a1-10 (Znt) transporters that remove Zn from the cytosol, the Fe exporter Ferroportin (Slc40a1), and Cu transporters Atp7a and Ctr1/2 (Slc31a1/2). Also shown are metallothioneins which store and buffer cytosolic Zn, and the Fe storage protein ferritin (Fth1 – ferritin heavy chain and Ftl1– ferritin light chain), which is protective against Fe-induced oxidative stress in macrophages.

Infection of 129S6 BMDMs leads to broad changes in genes that control metal transport (**Fig 5B, Supplementary Dataset S3**). There is a significant increase in *slc11a1* upon infection, particularly at 18 Hrs. Slc11a1 localizes to the phagosomal membrane where it exports divalent metal cations (Fe, Zn, Mn) while simultaneously acidifying the compartment. The other

bioRxiv preprint doi: https://doi.org/10.1101/2021.03.18.436026; this version posted March 18, 2021. The copyright holder for this preprint (which was not certified by peer review) is the author/funder, who has granted bioRxiv a license to display the preprint in perpetuity. It is made available under aCC-BY 4.0 International license.

member of this family, Slc11a2, imports metal ions across the plasma membrane, and is significantly upregulated at 2 Hrs. This may indicate an acute phase emphasis on importing metals into the cell, and a late phase emphasis on exporting metals from the phagosome. At 18 Hrs *slc11a1* is more highly expressed in response to live versus HK *Salmonella*, suggesting that macrophages actively upregulate this gene to help combat live infection.

There are also significant changes in transporters dedicated to import, export, and distribution of Fe, Cu and Zn **(Fig 5B)**. There is a downregulation of the transferrin (*trf*) Fe import pathway and the Fe exporter *slc40a1*, indicating restriction of Fe. The Cu transporters *slc31a1* (plasma membrane) and *slc31a2* (endosome) are significantly increased in expression at 18 Hrs. These changes in gene expression would increase Cu influx into the cytosol, while the upregulation of *atp7a* (endosome) at 2 Hrs suggests an active effort by the macrophages to kill the internalized bacteria. Changes in Zn transporters include upregulation of *slc30a4*, *slc39a14*, *slc39a1*, *slc39a7* and downregulation of *slc30a5*. The significant increase in expression of plasma membrane importer *slc39a14* is especially strong at 18 Hrs, and could result in an increase in cytosolic Zn. Decreased expression of Golgi importer *slc30a5* and increased expression of ER exporter *slc39a7* suggest diminished Zn in the secretory pathway, perhaps to deprive the pathogen of Zn. *Slc30a4*, which transports Zn into the phagosome and secretory vesicles, is upregulated at 2 Hrs and downregulated below control at 18 Hrs, indicating restriction of Zn at late stages of infection. Combined, there are widespread changes in metal transport that indicate limitation of Fe, accumulation of Cu, and redistribution of Zn.

In addition to metal transport, there are significant changes in genes that are metal dependent (**Fig 5C**) and genes related to metal homeostasis (**Fig 5D**). There is an increase in

bioRxiv preprint doi: https://doi.org/10.1101/2021.03.18.436026; this version posted March 18, 2021. The copyright holder for this preprint (which was not certified by peer review) is the author/funder, who has granted bioRxiv a license to display the preprint in perpetuity. It is made available under aCC-BY 4.0 International license.

intracellular storage capacity for Fe at 18 Hrs**;** *fth1* increases while *ftl1* drops in expression, reflecting the fact that during infection, heavy chains polymerize together to the exclusion of light chains(40). Similarly, Zn buffering capacity in the form of cytosolic metallothioneins (*mt1/2*) is increased early in infection and maintained with expression at 18 Hrs higher in macrophages treated with live versus HK *Salmonella*. These changes in metallothionein would be consistent with increased cytosolic Zn late in infection. There is also a significant increase in expression of Zn-dependent carbonic anhydrases that regulate pH, Zn-dependent proteases (*mmp10*, *12, 13, 14, timp1, adamts1, adam8*), the ferroxidase ceruloplasmin (**Fig 5C**). Additionally, there is an increase in expression of lipocalin, a protein involved in innate immunity by binding Fe-bound siderophores and depriving pathogens of Fe. Finally, there are significant increases in genes involved in metal homeostasis and oxidative stress, particularly at late stages of infection. These include: *hif1a*, Cu/Zn-dependent *sod2* and *sod3*, Mn-dependent *arg1*, and Zn-dependent *nos2*. These changes indicate that remodeling metal transport is accompanied by significant changes in the expression of metal-dependent enzymes and metal storage.

Cytosolic labile Zn increases at late stages of infection

The widespread changes in Zn transporter expression upon infection suggest remodeling of Zn homeostasis, and would be expected to lead to an increase in cytosolic Zn and decreased Zn in the secretory pathway. Previous studies in different model systems have suggested different changes in intracellular labile Zn pools in response to infection(27,41). However, all previous studies have used small molecule indicators such as FluoZin3 or Zinpyr-1,

bioRxiv preprint doi: https://doi.org/10.1101/2021.03.18.436026; this version posted March 18, 2021. The copyright holder for this preprint (which was not certified by peer review) is the author/funder, who has granted bioRxiv a license to display the preprint in perpetuity. It is made available under aCC-BY 4.0 International license.

317 which often exhibit variable and unpredictable localization within a cell and can confound
318 measurement of Zn in a defined location. For example, FluoZin3-AM has been shown to
319 localize to the cytosol, Golgi, lysosomes and vesicles, and localizations differ among cell
320 types(10,42,43). Previous studies in Slc11a1 defective Raw264.7 cells used FluoZin3 to
321 determine that there was an increase in labile Zn upon infection via FACS. Unfortunately, the
322 absence of fluorescence images precluded evaluation of where the Zn increase occurred. In
323 human monocyte-derived macrophages FluoZin3 appears to be in vesicles or early
324 endosomes(27), and reported an increase in Zn in these compartments upon infection. Of the
325 studies that have attempted to measure Zn inside activated or infected macrophage, none have
326 unambiguously addressed whether there are changes in cytosolic Zn.
327 To directly measure cytosolic Zn in 129S6 BMDMs at various time points post-infection,
328 we used the genetically encoded zinc sensor NES-ZapCV2(44,45). This sensor uses the ratio of
329 YFP emission to CFP emission upon CFP excitation (Forster Resonance Energy Transfer, FRET,
330 ratio) to measure labile Zn in cells. The advantage of the genetically encoded sensor is that
331 localization of this sensor is restricted to the cytosol. Briefly, cells were nucleofected with a
332 plasmid encoding NES-ZapCV2 15 hours prior to infection with *Salmonella*. At select time
333 points post-infection cells were imaged on a widefield fluorescence microscope to measure the
334 resting FRET ratio (**Fig 6A**). Cells were subsequently subjected to an *in situ* calibration to
335 determine the minimum and maximum FRET ratio in each cell (**Fig 6B**) and the calibration
336 parameters were used to calculate the fractional saturation of each cell under resting
337 conditions and the concentration of labile cytosolic Zn (see Methods for details, **Fig 6C**).
338 Uninfected cells have a mean fractional saturation of 0.30 which corresponds to a Zn

bioRxiv preprint doi: https://doi.org/10.1101/2021.03.18.436026; this version posted March 18, 2021. The copyright holder for this preprint (which was not certified by peer review) is the author/funder, who has granted bioRxiv a license to display the preprint in perpetuity. It is made available under aCC-BY 4.0 International license.

339 concentration of 80 pM. At 12 Hrs and beyond, the fractional saturation increased to ~ 0.5
340 which corresponds to ~ 2.9 nM Zn. Our data show that labile Zn in the cytosol does indeed
341 increase later in the infection (36-fold), consistent with the observed increase in expression of
342 *mt1* and *mt2*.
343
344 **Zn promotes bacterial clearance as well as bacterial replication**
345 Having established that Zn regulation and Zn availability in the cytosol are altered upon
346 infection, we evaluated the influence of Zn availability on infection outcome. While a previous
347 study examined increases and decreases in Zn on *Salmonella* infection of Raw264.7 cells(26),
348 we explore the impact of Zn on infection outcome in immune competent macrophages with
349 functional Slc11a1. To examine infection outcomes, we incorporated the pDiGc plasmid (**Fig 7A**)
350 into *Salmonella*, which encodes two fluorescent proteins. DsRed is expressed under an
351 arabinose inducible promoter while GFP is constitutively expressed(46). This plasmid allows
352 tracking of infected cells (green signal) and bacterial replication (dilution of the red signal upon
353 cell division). Arabinose induction of DsRed is halted upon macrophage infection, such that any
354 bacterial division occurring within the macrophage leads to dilution of the red fluorescent
355 signal. Comparison of green and red signals across time yields a picture of bacterial division vs
356 macrophage clearance of bacteria.
357 To alter Zn availability, we manipulated Zn levels in the macrophage media after
358 *Salmonella* had been internalized. Four media conditions were used in this study to span the
359 range from Zn replete to Zn deficient. The four conditions were: standard macrophage growth
360 media (DMEM + 20% FBS) containing 25 μM Zn (**Fig 7B**), or media prepared with Chelex-100-

bioRxiv preprint doi: https://doi.org/10.1101/2021.03.18.436026; this version posted March 18, 2021. The copyright holder for this preprint (which was not certified by peer review) is the author/funder, who has granted bioRxiv a license to display the preprint in perpetuity. It is made available under aCC-BY 4.0 International license.

361 treated FBS to deplete metal ions (4 μM Zn**, Fig 7B**), which was then further depleted of Zn
362 (Chelex media + 3 μM ZX1, ~ 0 μM Zn) or reconstituted with replete Zn (Chelex media + 30 μM
363 Zn, 34 μM Zn total).

364 Macrophages were infected with *Salmonella* expressing pDiGc in macrophage growth
365 media and infection proceeded for 45 minutes before experimental media conditions were
366 introduced. This avoided the confounding variable of Zn's effect on the phagocytosis of
367 bacteria. Infected macrophages in each media condition were fixed at four time points: 2, 10,
368 18 and 24 Hrs post inoculation and subjected to flow cytometry. A control sample was fixed
369 immediately after the 45 min infection and verifies that 91% of macrophages contained GFP-
370 positive bacteria at the beginning of the experiment. **Fig 7C** demonstrates the loss of GFP signal
371 in macrophages in each growth media as a function of time. The increase in the fraction of cells
372 with no GFP is indicative of bacterial clearance. In each panel, the white curve is from the initial
373 infection, and increased color saturation indicates time post-infection. In normal growth media,
374 clearance of bacteria is strong at 2 Hrs, with 70% of initially infected cells having lost all GFP
375 signal. Clearance further increases over time, with 76%, 74%, and 85% clearance at 10, 18 and
376 24 Hrs. Control and Zn replete media contained similar Zn levels but different amounts of Ca
377 and Fe due to Chelex treatment. At early time points (2, 10 and 18 Hrs) there is 56%, 64% and
378 59% bacterial clearance in the Zn replete media compared to the control, likely due to either
379 depleted Ca or Fe. By 24 Hrs, Zn replete samples reached a similar level of infection clearance,
380 with 87% clearance. In contrast, macrophages in Chelexed media with low Zn and ZX1-treated
381 media with effectively no Zn show significantly impaired bacterial clearance. At 24 Hrs Chelex
382 and Zx1 conditions had achieved 73% and 53% clearance, respectively. Direct comparison of the

bioRxiv preprint doi: https://doi.org/10.1101/2021.03.18.436026; this version posted March 18, 2021. The copyright holder for this preprint (which was not certified by peer review) is the author/funder, who has granted bioRxiv a license to display the preprint in perpetuity. It is made available under aCC-BY 4.0 International license.

different media conditions at each time point are presented in **Supplementary Figure S6**. These results confirm that 129S6 macrophages are competent at clearing *Salmonella* throughout infection and that Zn availability positively correlates with the effectiveness of bacterial clearance.

In addition to measuring bacterial clearance, the pDiGc plasmid can also be used to measure bacterial replication, as the DsRed signal is diluted with every cell division. We compared the DsRed signal versus GFP signal as a function of time and different media conditions (**Fig 8**). In standard macrophage growth media (top row), the DsRed signal decreases over time in 23% of the GFP+ cells, indicative of bacterial replication. It is important to note that although 129S6 macrophage are efficient at clearing the *Salmonella* infection, here we are looking at the small portion of the macrophage population that remains infected (GFP^+). The Zn replete media (2^{nd} row) shows bacterial replication comparable to standard growth media, with 23% of GFP^+ macrophages showing diluted DSRed signal at 24 Hrs. In contrast, in Chelexed media with depleted Zn and Chelexed media containing ZX1 (no Zn) there is weaker bacterial replication (11% and 7%, respectively), as indicated by the lack of a fluorescent "tail" at lower DsRed intensity. Interestingly, this result suggests that while Zn facilitates host clearance of bacteria, it also helps bacteria to replicate in cells that do not clear the infection. This may suggest that bacterial clearance occurs more easily in dividing bacteria as persistent infections are mainly non-replicating.

Macrophages from 129S6 and C57BL/6 differ in nutritional immune response to infection

bioRxiv preprint doi: https://doi.org/10.1101/2021.03.18.436026; this version posted March 18, 2021. The copyright holder for this preprint (which was not certified by peer review) is the author/funder, who has granted bioRxiv a license to display the preprint in perpetuity. It is made available under aCC-BY 4.0 International license.

Because the Slc11a1 transporter specifically aids in depriving pathogens of metal ions, we hypothesized that expression of genes related to metal handling in our cells would differ significantly from macrophages derived from Slc11a1 non-functional mice (BALB/c, C57BL/6, and the Raw264.7 cell line). Therefore, we performed a comprehensive analysis of changes in expression in 129S6 macrophages (this study) and macrophages derived from C57BL/6 mice (RNAseq study by Stapels et al(47)) at 18 hours post infection. Specifically, we compared our unexposed control (UE), 18 Hr Alive and 18 Hr HK conditions against uninfected macrophages (UI), those containing growing *Salmonella* (G), and bystander macrophages not containing *Salmonella* at 18 Hrs (BY) from Staples et al. All data were analyzed on the same pipeline and normalized together within DESeq2 to make the data as comparable as possible **(Supplementary Dataset S4)**.

To evaluate potential differences in genes involved in nutritional immunity between the two datasets, we examined all genes with UNIPROT keywords for iron, zinc, or copper transport or homeostasis. **Fig 9** presents heat maps for Fe, Cu, Zn transport and Ze-dependent genes. There are a number of similarities in regulation of metal-transport, -homeostasis, and -dependent genes, indicating that there are common mechanisms for managing metal ions at the host-pathogen interface, even when there are differences in the host. In particular, there is a significant decrease in Fe import (*trf*), export (*slc40a1*), and an increase in ferritin storage (*fth1*) in both studies (**Fig 9A**). Similarly, both studies show upregulation of plasma membrane copper transporter *slc31a1* indicating Cu uptake from the extracellular space (**Fig 9B**). With respect to Zn regulation, both studies show upregulation of plasma membrane Zn importer *slc39a14*, downregulation of the Golgi importer *slc30a5*, and an increase in expression of Zn

bioRxiv preprint doi: https://doi.org/10.1101/2021.03.18.436026; this version posted March 18, 2021. The copyright holder for this preprint (which was not certified by peer review) is the author/funder, who has granted bioRxiv a license to display the preprint in perpetuity. It is made available under aCC-BY 4.0 International license.

426 buffers *mt1* and *mt2* (**Fig 9B, 9C**). Combined these results suggest a general pattern of limiting
427 the availability of Fe, increasing exposure to Cu, and increasing cytosolic Zn.

428 Despite these similarities, there are also notable differences that suggest the presence
429 of functional *slc11a1* alters metal regulation at the host-pathogen interface. With respect to
430 Fe, lactotransferrin (*ltf*), a major Fe binding factor with bactericidal properties, *steap3*, which
431 encodes a ferrireductase that reduces ferric Fe released from transferrin in the endosome, and
432 *mmgt1*, which encodes a Mg transporter that ferries multiple metal ions across membranes are
433 all downregulated in infected 129S6, but do not respond to infection in C57BL/6 cells. There are
434 also notable differences in key Cu regulatory genes. The Cu importer *slc31a2* is upregulated in
435 129S6, while there is no change in C57BL/6. Copper chaperones play an important role in
436 distributing Cu and loading it into enzymes; the copper chaperone *atox1* is upregulated in
437 129S6, but downregulated in C57BL/6; *cox17* is upregulated in 129S6, but not C57BL/6 ($q > 0.06$).
438 Finally, *sco1* is upregulated in C57BL/6 but not 129S6. There are also differences in the
439 magnitude of gene expression changes, with more marked changes in 129S6, including for
440 ferroportin (*Slc40a1*), multi-copper enzyme ceruloplasmin (*cp*), and *lcn2*, which reduces
441 bacterial replication by sequestering Fe bound to microbial siderophores. *Lcn2* is also intimately
442 involved in regulating the expression of pro-apoptotic *bcl2l11,* which is strongly downregulated
443 in 129S6 but is unaffected in C57BL/6 cells, suggesting these two cell types have disparate
444 apoptotic tendencies at 18 Hrs post infection.

445 There are also notable differences in infection-induced expression changes in genes
446 encoding Zn transporters and Zn-dependent proteins between the two systems (**Fig 9C, D**).
447 Specifically, upregulation of *slc39a7* and downregulation of *slc30a4* in 129S6 but not C57BL/6

bioRxiv preprint doi: https://doi.org/10.1101/2021.03.18.436026; this version posted March 18, 2021. The copyright holder for this preprint (which was not certified by peer review) is the author/funder, who has granted bioRxiv a license to display the preprint in perpetuity. It is made available under aCC-BY 4.0 International license.

suggest limitation of Zn in the secretory pathway and phago-lysosomal compartment in response to infection in 129S6 BMDMs. Additionally, *slc39a8* is downregulated in 129S6 but upregulated in C57BL/6. In primary human lung macrophages, the Zn importer *slc39a8* is upregulated in response to LPS and negatively regulates proinflammatory responses(48). Zn-dependent proteins such as proteases (*mmp9/10/12/13*) and carbonic anhydrases (*car 4/11*), are upregulated in 129S6 but not C57BL/6. Finally, there are notable differences in the magnitude of gene expression changes, including *car2*, *car4*, and *nos2*. These differences suggest changes in Zn distribution between the two model systems and altered regulation of Zn-dependent enzymes.

A comparison between A18 vs UE and G vs UI revealed global expression differences as well. 1991 genes are differentially expressed (padj < 0.01) between G and UI that were not differential (padj > 0.03) between A18 and UE. Further, 2723 genes were significantly different between A18 and UE, but not in G versus UI. When these gene lists were scrutinized using DAVID annotation clustering, the genes differential in 129S6 were enriched for cell cycle functions, and the majority are down regulated. Interestingly, the genes differentially expressed in C57BL/6 were enriched for apoptosis, and almost all of these genes were upregulated. These data suggest that these two cell types are moving toward different fates by 18 Hrs post *Salmonella* exposure, with 129S6 cells entering quiescence but C57BL/6 cells experiencing apoptosis. This observation is consistent with the fact that Slc11a1 knockout macrophages are models for acute infection and are more susceptible to killing by *Salmonella*.

Discussion

bioRxiv preprint doi: https://doi.org/10.1101/2021.03.18.436026; this version posted March 18, 2021. The copyright holder for this preprint (which was not certified by peer review) is the author/funder, who has granted bioRxiv a license to display the preprint in perpetuity. It is made available under aCC-BY 4.0 International license.

This work presents a systematic analysis of changes in global gene expression, as well as a more targeted analysis of changes in genes related to transition metal ions in 129S6 macrophages infected with *Salmonella*. The 129S6 model system was chosen because these mice contain functional Slc11a1 (Nramp1), a divalent metal ion transporter that localizes to phagosomes and regulates metal availability to the intracellular pathogen. Slc11a1 confers resistance to intracellular pathogens and the 129S6 mouse has been used to model long-term chronic infection by *Salmonella*, as the mice don't succumb to initial acute infection the way C57BL/6 or BALB/c mice do(30,49,50). A recent study examined the *Salmonella* proteome upon infection of mice homozygous or heterozygous for functional versus nonfunctional Scl11a1 and found an abundance of Mg, Zn, Fe and Mn uptake systems expressed in *Salmonella* in resistant mice but not *Salmonella* that colonized susceptible BALB/c mice(49). This study indicates that Slc11a1 plays a major role in affecting metal ion availability for uptake by *Salmonella*. However, how metal regulation in the host differs in the presence and absence of functional Slc11a1 has not been explored. Given that metal manipulation is a key component of nutritional immunity, we sought to define how genes encoding metal transporters, metal-dependent proteins, and metal-regulatory proteins were affected by treatment with live or heat killed *Salmonella* at early (2 Hrs post infection) and late (18 Hrs post infection) time points.

We observed widespread changes in metal transport, metal-dependent, and metal homeostasis genes, suggesting remodeling of Fe, Cu, and Zn availability by host cells. There is significant upregulation of *slc11a1*, especially at late stages of infection, consistent with the host cell limiting Fe, Mg, Mn and Zn in the phagosome. Further changes in gene expression are consistent with decreased Fe uptake (*trf*), export (*slc40a1*) and increased storage (*fth1*);

bioRxiv preprint doi: https://doi.org/10.1101/2021.03.18.436026; this version posted March 18, 2021. The copyright holder for this preprint (which was not certified by peer review) is the author/funder, who has granted bioRxiv a license to display the preprint in perpetuity. It is made available under aCC-BY 4.0 International license.

492 increased Cu uptake (*slc31a1*), import into the phagosome (*atp7a*) and altered distribution (Cu
493 chaperones *atox1, sco1, cox17*) and increased transport of Zn into the cytosol (*slc39a1*,
494 *slc39a14*) coupled with decreased transport into the secretory pathway and endo-lysosomal
495 system (*slc39a7, slc30a4, slc30a5*). Increased expression of *mt1* and *mt2* genes, which encode
496 Zn buffering proteins, further suggests an increase in cytosolic Zn. We also observed numerous
497 changes in metal-dependent proteins and enzymes, many of which play an important role in
498 nutritional immunity (*lcn2, ltf, cp, steap3, sod2, arg1, nos2, mmp, car, s100a8*). Some of these
499 changes have been seen in a variety of mouse model systems in response to diverse
500 intracellular pathogens, suggesting widespread or universal strategies for the host to combat
501 infection. In particular, the changes in gene expression to limit Fe(6,51) and accumulate Cu
502 appear to be common strategies for nutritional immunity(4). Indeed, the changes in expression
503 of *trf, slc40a1, fth1, slc31a1, lcn2* and *cp* were also observed in analysis of RNAseq data from
504 infection of macrophages from C57BL/6 mice at 18Hrs post infection. However, it is notable
505 that many of the changes are significantly more pronounced (larger fold change) in the 129S6
506 model system, indicating a more robust nutritional immunity response in macrophages with
507 functional Slc11a1. This observation is consistent with the findings of Cunrath and Bumann,
508 which found that only in infection of mice with functional Slc11a1 were bacterial metal uptake
509 systems induced(49), suggesting that functional Slc11a1 is necessary to activate nutritional
510 immunity mechanisms. Interestingly, the changes we observed in expression in *slc11a1*, as well
511 as key Fe and Cu regulatory genes were comparable in macrophages infected with live bacteria
512 or treated with HK bacteria. This suggests that the host response is driven not only by active
513 pathogen virulence factors, but also pathogen-associated cues, such as LPS.

bioRxiv preprint doi: https://doi.org/10.1101/2021.03.18.436026; this version posted March 18, 2021. The copyright holder for this preprint (which was not certified by peer review) is the author/funder, who has granted bioRxiv a license to display the preprint in perpetuity. It is made available under aCC-BY 4.0 International license.

As noted previously, there does not appear to be a universal strategy for host manipulation of Zn at the host-pathogen interface, with examples of host mechanisms to both starve and poison an intracellular pathogen(2,5,22). Cellular regulation of Zn is more complex than Fe or Cu, with 24 Zn transporters that control transport into and out of the cytosol as well as intracellular organelles. Indeed, pathogens and immune system modulators have been shown to have different effects on Zn transporter expression(7) including upregulation of *slc39a8*(48) in response to LPS and TNFα, upregulation of *slc30a4* and *slc30a7* upon stimulation with GM-CSF(52), and upregulation of *slc39a14* in response to LPS(53). Previous studies have suggested that *Salmonella* experiences Zn starvation inside the host as the high affinity bacterial Zn uptake system ZnuABC(23) and associated accessory protein ZinT(24) and low affinity uptake system ZupT(54) contribute to virulence in mice. But the concept of Zn starvation is hard to reconcile with reports of Zn accumulation in puncta(27) and the suggestion that *Salmonella* induce Zn elevation to evade bacterial clearance(26). To provide a more complete picture of Zn modulation within the host, we analyzed changes in the expression of Zn regulatory genes, measured labile Zn levels in the cytosol at different times post infection, and examined the effect of Zn availability (based on manipulation of Zn levels in media) on infection outcomes: bacterial clearance and bacterial replication. We were particularly interested in comparing how the host cell remodels Zn availability in macrophages with functional Slc11a1, and hence a robust nutritional immunity response.

The changes in Zn transporters and homeostasis genes predict an increase in cytosolic Zn and a decrease in Zn in the ER / Golgi / phagosome. Specifically, we observed significant upregulation of *slc39a1*, *slc39a14*, *mt1* and *mt2*, with more pronounced changes at late stages

bioRxiv preprint doi: https://doi.org/10.1101/2021.03.18.436026; this version posted March 18, 2021. The copyright holder for this preprint (which was not certified by peer review) is the author/funder, who has granted bioRxiv a license to display the preprint in perpetuity. It is made available under aCC-BY 4.0 International license.

of infection (18 Hrs). Slc39a1 and a14 are plasma membrane transporters that mediate entry of Zn into the cytosol, while Mt1 and Mt2 are Zn buffering proteins that are frequently used as proxies for cytosolic Zn, as increased Zn leads to increased *mt1/2* expression via the Zn-dependent transcription factor Mtf1. Using a genetically encoded Zn sensor explicitly targeted to the cytosol, we measured an increase in Zn from ~ 80 pM to ~ 2 nM at 12 Hrs post infection that remained elevated through the last measurement time (21 Hrs post infection). Intriguingly, *mt1*, *mt2*, and *slc39a14* are more highly upregulated upon infection with live *Salmonella* compared with heat killed bacteria, suggesting an active recognition of and response to live bacteria. We speculate that the host cell increases cytosolic Zn to support metabolic and transcriptional proteins that fight infection. This is consistent with our observation that a large fraction of differentially expressed genes has DAVID annotations that include “Zn binding”. When we manipulated Zn availability in the media, we found that Zn replete conditions led to robust clearance of infected bacteria, suggesting that the host may use elevated cytosolic Zn to fight infection.

We also observed an increase in *slc39a7* which encodes the transporter that moves Zn out of the ER and secretory pathway, a decrease in *slc30a5* which encodes the transporter that moves Zn into the Golgi and vesicular compartments, and a decrease in *slc30a4* which encodes a transporter which moves Zn into the phagosome. All three of these changes were comparable in macrophages treated with live *Salmonella* versus heat HK bacteria, suggesting a general host response to the pathogen and pathogen-associated cues (for example LPS). Further, all three of these changes in expression would lead to Zn limitation in the secretory / phago/lyoso-somal pathway and hence Zn restriction for the pathogen. This finding is

bioRxiv preprint doi: https://doi.org/10.1101/2021.03.18.436026; this version posted March 18, 2021. The copyright holder for this preprint (which was not certified by peer review) is the author/funder, who has granted bioRxiv a license to display the preprint in perpetuity. It is made available under aCC-BY 4.0 International license.

558 consistent with previous observations that *Salmonella* upregulate bacterial Zn uptake
559 mechanisms, especially in the presence of functional Slc11a1. Manipulation of Zn in the media
560 revealed that zinc availability strongly correlated with bacterial replication, where Zn limitation
561 blocked replication and Zn elevation enabled replication. Combined, our results indicate that
562 manipulation of Zn at the host-pathogen interface is more nuanced than Fe or Cu, where the
563 host leverages its intricate means of manipulating Zn availability and distribution to limit the
564 ability of the pathogen to access Zn while simultaneously ensuring sufficient Zn to support the
565 immune response.

566 In addition to representing a distinct model system for studying nutritional immunity,
567 we anticipated that the presence of functional Slc11a1 would affect the global immune
568 response to infection, since Slc11a1 profoundly affects infection outcomes, namely resistance
569 versus susceptibility. To critically compare infection-induced changes in the transcriptome, we
570 identified an RNAseq study that was carried out in macrophages from C57BL/6 mice(47), with
571 strong parallels to our conditions, and reanalyzed the data along with ours in an identical
572 pipeline. We found that 4500 genes were differentially expressed in one study but not the
573 other, with differences in expression at baseline as well as in response to infection. This is
574 consistent with studies of mouse lines possessing one or two functional *slc11a1* alleles on a
575 C57BL/6 background(30,49). These mice experienced lower infection loads but still ultimately
576 succumbed to *Salmonella* infection, implying differences between C57BL/6 mice and 129S6
577 mice that extend beyond Slc11a1. However, the magnitude of differential expression was
578 unexpected, as it involved more than a third of all genes differentially expressed in our data.
579 Annotation analysis of this differential gene list indicates that these cell types tend toward

bioRxiv preprint doi: https://doi.org/10.1101/2021.03.18.436026; this version posted March 18, 2021. The copyright holder for this preprint (which was not certified by peer review) is the author/funder, who has granted bioRxiv a license to display the preprint in perpetuity. It is made available under aCC-BY 4.0 International license.

different fates in response to the stress of *Salmonella* infection, with 129S6 cells showing suppression of cell cycle genes but C57BL/6 cells showing upregulation of apoptotic genes.

In assessing the GSEA and GO term enrichment present in our data we find recurring themes of inflammation, hypoxia, apoptosis and the unfolded protein response (UPR), which are inextricably linked(36,55). Both intracellular hypoxia and *Salmonella*-induced inflammation can result in apoptosis or the UPR, which is an attempt to regain cellular homeostasis under stress. When comparing live vs HK *Salmonella* conditions across time, we see enrichment of hypoxia-related genes along with enrichment of apoptosis 2 Hrs, which transitions to enrichment of UPR at 18 Hrs. This apparent transition in the cellular stress response over time demonstrates the ability of 129S6 macrophages to withstand *Salmonella* infection. In contrast, infection of C57BL/6 macrophages showed marked enrichment of apoptosis genes at 18 Hrs. This finding is supported by multiple previous studies which found that *Salmonella* induces apoptosis in Slc11a1 nonfunctional macrophages(39,56).

Macrophages experience a range of phenotypes, from inflammatory and cytotoxic (termed M1 polarization) to anti-inflammatory and wound healing (M2 polarization), depending on their milieu. These states are fluid, differing in gene expression and metabolism, and are heterogeneous across *in vivo* cell populations(36). The bactericidal mechanisms available to M1 macrophages enable them to kill internalized pathogens efficiently. The lack of these mechanisms in M2-like macrophages make them a more permissive niche for facultative intracellular bacteria like *Salmonella*. Although a number of previous studies have tried to identify individual genes that distinguish M1 and M2, for example: *arg1* vs *nos2*(57) or *egr2* vs *CD38*(58), the increasing availability of whole transcriptome sequencing makes it possible to

bioRxiv preprint doi: https://doi.org/10.1101/2021.03.18.436026; this version posted March 18, 2021. The copyright holder for this preprint (which was not certified by peer review) is the author/funder, who has granted bioRxiv a license to display the preprint in perpetuity. It is made available under aCC-BY 4.0 International license.

602 define a more comprehensive genetic signature of M1 and M2. Single cell RNAseq by Saliba et
603 al(31) enabled identification of gene clusters related to M1 and M2 and how these gene
604 clusters correlated with infection (naïve macrophages, bystanders, macrophages with growing
605 bacteria and macrophages with non-growing bacteria). Dual RNAseq of both the pathogen and
606 host by Stapels et al(47) further enables correlation of the M1 and M2 gene clusters within the
607 host with expression of *Salmonella* virulence genes. Indeed, this analysis revealed that in
608 C57BL/6 macrophages, the M2 polarization correlates with increased SPI2 expression,
609 suggesting that *Salmonella* activates virulence mechanisms in this niche.
610 Examination of M1 and M2 gene clusters further reinforces that 129S6 macrophages
611 represent a distinct intracellular niche with respect to immune response to infection. As shown
612 in **Fig 2**, polarization genes follow a temporal pattern of expression, with the majority of M1
613 related genes strongly upregulated 2 Hrs post infection but sharply downregulated by 18 Hrs.
614 On the other hand we see slower time-dependent activation of M2 related genes. This
615 observation is supported at 2 Hrs by enrichment in glycolysis, the metabolic state of
616 inflammatory or hypoxic macrophages, and at 18 Hrs by enrichment in oxidative
617 phosphorylation and fatty acid metabolism, which are the metabolic markers of M2
618 macrophages(36,55). Importantly, at each time point we see little difference in M1/M2
619 associated genes between live and HK *Salmonella* conditions, especially when normalized to
620 C57BL/6 data **(Supplementary Figure S7)**. This is in contrast to findings in Slc11a1 non-
621 functional macrophages which indicate that dividing *Salmonella* may actively induce M2
622 polarization to enhance bacterial survival, and that macrophages exposed to but not infected
623 by *Salmonella* maintain an M1 phenotype late in infection(31,47). While our work is at a

bioRxiv preprint doi: https://doi.org/10.1101/2021.03.18.436026; this version posted March 18, 2021. The copyright holder for this preprint (which was not certified by peer review) is the author/funder, who has granted bioRxiv a license to display the preprint in perpetuity. It is made available under aCC-BY 4.0 International license.

624 population level and therefore contains macrophage and *Salmonella* heterogeneity, exposure
625 to HK Salmonella does not lead to retention of an M1 phenotype at 18 Hrs, nor does it seem
626 that 129S6 cells are induced to M2 by live *Salmonella*.

627 Our study recapitulates the ability of 129S6 macrophages to fight infection at all time
628 points, which intriguingly occurs regardless of the expression profile of M1 or M2 genes. At 2
629 Hrs, 70% of initially infected macrophages had cleared the infection, which correlated with the
630 transcriptional induction of M1 polarization. However, despite the shift toward an M2-like
631 transcriptional profile at 18 Hrs, the rate of bacterial clearance increased slightly over time to
632 74%. Concurrently the proportion of infected macrophages showing evidence of bacterial
633 replication also increased over time, from 8% at 10 and 18 Hrs to 24% by 24 Hrs. This high
634 clearance rate and relatively low replication rate resulted in only 3% of initially infected
635 macrophages harboring dividing bacteria at 24 Hrs **(Supplementary Dataset S5)**. This is in
636 contrast to studies of Nramp1$^{+/+}$ 129X1 mice(59) and Slc11a1 nonfunctional macrophages which
637 report that replicating *Salmonella* are preferentially found in M2 cells(31,35,47). It is also
638 notable that 129S6 macrophages surviving to 24 Hrs while harboring dividing *Salmonella* are
639 not allowing high division rates, as indicated by only modest decreases in the inducible
640 fluorescent signal (**Fig 9**), whereas Slc11a1 nonfunctional macrophages experience high levels
641 of *Salmonella* division at 24 Hrs(35,46). It is important to note that Zn was a key factor in both
642 clearance and bacterial replication processes, as reduced zinc availability correlated with
643 attenuation of both.

644 This study reveals that 129S6 macrophages differs significantly from other model
645 systems of *Salmonella* infection which possess a nonfunctional Slc11a1. First, 129S6

bioRxiv preprint doi: https://doi.org/10.1101/2021.03.18.436026; this version posted March 18, 2021. The copyright holder for this preprint (which was not certified by peer review) is the author/funder, who has granted bioRxiv a license to display the preprint in perpetuity. It is made available under aCC-BY 4.0 International license.

macrophages show a robust remodeling of metal homeostasis and expression of metal-dependent enzymes, that indicate the nutritional immunity response within the host differs in the presence of functional Slc11a1. Second, remodeling of Zn regulatory proteins leads to an increase in cytosolic Zn and a likely restriction of Zn for the pathogen. This multi-pronged approach ensures sufficient cytosolic Zn to fight infection and promote bacterial clearance, while still limiting Zn availability to fight against bacterial replication. Third, transcription of M2-related genes doesn't correlate exclusively with live *Salmonella* exposure or with a lack of bactericidal capacity, suggesting that in this model system the M2 polarization does not promote bacterial survival. Rather, activation of M1-related genes early and M2-related genes at later time points correlates with the switch from expression of apoptosis genes to UPR genes and suggests a choreographed response to fight infection without killing the host cell. Together, these imply that 129S6 macrophages do not conform well to the M1/M2 expression dichotomy derived largely from Nramp1 nonfunctional macrophages and mice. Instead, they appear to present a mixed phenotype that effectively uses zinc to quell *Salmonella* infection.

Materials and Methods

Ethics statement

This study was approved by the Institutional Animal Care and Use Committee at University of Colorado Boulder. The animal subjects plan protocol number is 2547.

Monocyte extraction from bone marrow

Animal work followed protocol 2547, approved by University of Colorado IACUC. 8-12 week-old 129S6 female mice (Taconic Laboratories) were euthanized by CO_2 inhalation

bioRxiv preprint doi: https://doi.org/10.1101/2021.03.18.436026; this version posted March 18, 2021. The copyright holder for this preprint (which was not certified by peer review) is the author/funder, who has granted bioRxiv a license to display the preprint in perpetuity. It is made available under aCC-BY 4.0 International license.

668 according to IACUC guidelines, followed by cervical dislocation. Femur, tibia and humerus
669 bones were extracted, then scraped and flushed with ice cold phosphate buffered saline (PBS).
670 Approximately 1 mL of PBS was used per bone. PBS with marrow cells was passed through a 70
671 micron nylon mesh Falcon™ Cell Strainer (Corning™ 352350), then overlaid onto an equal
672 volume of Histopaque-1083 (Sigma-Aldrich) in centrifuge tubes. Tubes were centrifuged at 500
673 x G for 30 min and allowed to slow with no brake. Monocytes appear as a fuzzy layer at the
674 fluid interface. These were removed to clean tubes and washed twice with 14 mL PBS. After the
675 final wash monocytes were resuspended in a small amount of macrophage growth media and
676 counted with a hemocytometer. Growth media consisted of DMEM (Sigma-Aldrich)
677 supplemented with 20 % fetal bovine serum (FBS), 2 mM L-glutamine, 1 mM sodium pyruvate,
678 penicillin/streptomycin (50 IU/mL penicillin and 50 μg/mL streptomycin) and 10 pg/μL
679 recombinant murine macrophage colony stimulating factor (PeproTech, Inc.).
680
681 **Primary cell culture and infection**
682 Monocytes were plated into 12-well plates at a density of 200,000 cells per well. 2 mL
683 macrophage growth media was added to each well and plates were incubated at 37 °C and 5%
684 CO_2 for 6 days. Media was refreshed 3 days after plating. Wild type *Salmonella* Typhimurium
685 SL1344 was cultured to stationary phase in LB with [antibiotics] at 37 °C with aeration. Bacteria
686 were washed with PBS and opsonized for 30 minutes at room temperature in a 1:1 solution of
687 mouse serum (Sigma) and cell culture media (Gibco). Bacteria were then pelleted at 13,000 x G
688 for 1 minute and resuspended in PBS. Half of the bacteria was heat killed at 60° C for 3 minutes,
689 then placed on ice. One well of macrophages was scraped and counted, and bacteria were

bioRxiv preprint doi: https://doi.org/10.1101/2021.03.18.436026; this version posted March 18, 2021. The copyright holder for this preprint (which was not certified by peer review) is the author/funder, who has granted bioRxiv a license to display the preprint in perpetuity. It is made available under aCC-BY 4.0 International license.

diluted in macrophage media without antibiotics to an MOI of 30. Plated macrophages were washed 3 times with PBS, then treated with antibiotic free macrophage media containing live, heat killed, or no bacteria. 30 minutes later bacterial media was removed, cells were washed 3x with PBS, and macrophage media containing 100 g/mL gentamicin was added. 90 minutes later media was again removed. RNEasy lysis buffer was added directly to wells designated as 2 Hr samples. Macrophage media with 10 μg/mL gentamicin was added to wells designated as 18 Hr samples. Lysed samples were collected and frozen at -20 °C. 18 Hrs post *Salmonella* exposure media was removed from remaining wells, lysis buffer was added, and cell lysates were frozen at -20 °C. To examine both early and late immune responses, macrophages were lysed at 2 or 18 hours post bacterial exposure. Control samples were lysed at the two-hour timepoint.

RNA extraction and sequencing

RNA extraction was done on all samples at once, after one freeze-thaw cycle. An RNEasy kit (Qiagen) was used, and DNAse I treatment was done on the column. RNA integrity was checked via Tape Station, and library prep was done with an Illumina TruSeq LT kit which included polyA selection. Paired end 75 base sequencing was done on a NextSeq 2.1.0 Illumina machine. Tape station run, library prep and sequencing were performed by the JSCBB sequencing core.

Data analysis pipeline

R 3.3.0 on the JSCBB computing core was used for analysis of raw data. Data quality was assessed with fastqc (0.11.2) and the first 10 bases were trimmed with Trimmomatic (0.36).

bioRxiv preprint doi: https://doi.org/10.1101/2021.03.18.436026; this version posted March 18, 2021. The copyright holder for this preprint (which was not certified by peer review) is the author/funder, who has granted bioRxiv a license to display the preprint in perpetuity. It is made available under aCC-BY 4.0 International license.

712 Reads were mapped with TopHat(2.0.6)/Samtools (0.1.18)/bowtie2 (2.0.2) using --b2-very-
713 sensitive, fr-firststrand settings. Read counting was completed with EdgeR Subread
714 featureCounts (1.6.0) using the mm10 gtf file from UCSC (July 2015 version). MetaFeature
715 mapping was paired end, with both ends mapped, and no MultiOverlap allowed. R 4.0.2 was
716 used for all remaining analysis. A principal component analysis (PCA) of global RNA expression
717 was performed using EdgeR. Analysis of differential expression was done with DESeq2 (1.18.1)
718 but the nature of this dataset violates the DESeq2 assumption that most genes do not change
719 expression between conditions. Therefore, all genes with differential expression padj < 0.05 in
720 binary comparisons were compiled and excluded from the final dds normalization using the
721 controlGenes parameter. A log ratio test on the correctly normalized DESeq dataset matrix
722 (dds) with the following function: DESeq(dds, test="LRT", reduced = ~ 1), and resulted in a list of
723 globally differentially expressed genes. This dataset ($p < 0.01$) was further filtered with two
724 Transcripts Per Million (TPM) requirements. Inclusion in the final analysis indicates that a gene
725 has an overall mean TPM > 5, and at least one condition with a mean TPM > 10. The 7766 genes
726 meeting these criteria were fed into DEGReport R package(1.24.1) for rlog transformation,
727 which produced normalized counts, and expression clustering, which produced Z-scores.
728 Expression clustering was done with the following function: degPatterns(cluster_rlog, metadata
729 = metadata, time = "Treatment").Heatmap gene dendrograms were constructed using
730 hierarchical clustering package hclust and ggdendro (0.1.22), and this gene order was used to
731 construct global and cluster heatmaps with ggplot (Tidyverse R package 1.3.0). The median
732 value for each plot was set as white. DAVID annotation enrichment categories were used to

bioRxiv preprint doi: https://doi.org/10.1101/2021.03.18.436026; this version posted March 18, 2021. The copyright holder for this preprint (which was not certified by peer review) is the author/funder, who has granted bioRxiv a license to display the preprint in perpetuity. It is made available under aCC-BY 4.0 International license.

assess the makeup of DEGReport clusters. This analysis included functional categories, Gene Ontology, Biocarta and Kegg pathways, and protein domains.

In brief, DESeq2 binary comparisons between conditions were fed into GSEA(60) to validate GO term enrichment and assess transcription targets. More specifically, adjusted p-value ranked lists were created from DESeq2 differential expression data sets comparing 2A vs. 2HK or 18A vs. 18HK. For each gene in a given data set, a rank was determined from the padj value (false discovery rate) and the direction of fold change value (up or down regulation). Rank = -log(padj) * sign(fold change). All genes with a valid padj value were included. GSEA was used to compare these ranked lists to validated gene sets. These were: Canonical Pathways, Hallmark gene sets, GO_Biological Processes, GO_Molecular Functions, and Transcription Factor Targets. Because GSEA's default is human gene sets, the mouse genome was collapsed and remapped using the Mouse Gene Symbol Remapping Human Orthologs MsigDB.v7.2.chip. Gene set permutations were used in this analysis, which is a less stringent assessment of significance, and produces more false positive results. Therefore, a cutoff of $q < 0.05$ was applied to gene set results.

Comparison of current study with Staples et al, Science, 2018

FASTQ files (GEO accession GSE104785) were downloaded and run through the above pipeline with the following alterations: Trimmomatic was used to remove Illumina adaptors, and alterations were made to mapping and counting based on the unstranded nature of the data. This differs from the pipeline of Staples et al. in that their data was mapped to the *Salmonella* genome prior to the mouse mm10 genome. Additionally, their read counts were

bioRxiv preprint doi: https://doi.org/10.1101/2021.03.18.436026; this version posted March 18, 2021. The copyright holder for this preprint (which was not certified by peer review) is the author/funder, who has granted bioRxiv a license to display the preprint in perpetuity. It is made available under aCC-BY 4.0 International license.

performed with HTSeq (version 0.6.1) instead of FeatureCounts. To normalize our data with this previously published dataset, DESeq2 was run on the combined data with the experimental design ~Treatment, and normalized counts were calculated. PCA and dendrogram of the Staples dataset were created and compared with their published heatmap to generally validate our sequencing results (**Supplementary Figure S8**).

To assess differences in metal homeostasis genes as comprehensively as possible, mouse specific lists of genes involved in the transport and homeostasis of metal ions were compiled from the Uniprot database. Separate lists were compiled for Zn, Fe, and Cu, and each list was compared against the normalized counts of the aggregated sequencing studies. Only genes expressed above background were used for further analysis.

Measurement of cytosolic Zn and Imaging analysis

For quantification of cytosolic labile Zn in primary macrophages, calibration experiments were performed at the indicated times post infection on a Nikon Ti-E widefield fluorescence microscope equipped with Nikon elements software, Ti-E perfect focus system, an iXon3 EMCCD camera (Andor), mercury arc lamp, and YFP FRET (434/16 excitation, 458 dichroic, 535/20 emission), CFP (434/16 excitation, 458 dichroic, 470/24 emission), and YFP (495/10 excitation, 515 dichroic, 535/20 emission) filter sets. External excitation and emission filter wheels were controlled by a Lambda 10-3 filter changer (Sutter Instruments), while dichroic mirrors were placed on cubes in the dichroic turret. Channel EM gain and exposure settings for both YFP FRET and CFP were set to be the same. Images were collected using a 60X oil objective (NA 1.40), 200 ms exposure time, EM gain 1 MHz at 16-bit readout mode with an EM

bioRxiv preprint doi: https://doi.org/10.1101/2021.03.18.436026; this version posted March 18, 2021. The copyright holder for this preprint (which was not certified by peer review) is the author/funder, who has granted bioRxiv a license to display the preprint in perpetuity. It is made available under aCC-BY 4.0 International license.

777 gain multiplier of 200, and a neutral density filter with 25% light transmission. Sensor
778 expression level was controlled by selecting cells with YFP intensities between 4,000-15,000
779 fluorescence units under these conditions. 8 fields of view were collected using multipoint
780 acquisition mode and the Perfect Focus System (PFS) set to 'ON' in between points. Cells were
781 maintained at 37°C and 5% CO2 in a LiveCell™ environment chamber (Pathology Devices)
782 during the experiments. Images were collected every minute during $R_{Resting}$ and R_{min} calibration
783 acquisition phases and every 30 seconds during the R_{max} calibration phase.

784 Fresh calibration solutions were prepared the day of the experiment and include a 2X
785 solution of R_{min} buffer (50µM TPA in PO_4^{3-}-free HHBSS) for minimum FRET ratio collection and a
786 2X solution of R_{max} buffer (0.001% saponin + 0.75 µM pyrithione + 23.8nM buffered Zn in PO_4^{3-}-,
787 Ca^{2+}-, Mg^{2+}-free HHBSS) for collecting the maximum FRET ratio. The resting FRET ratio of the
788 sensor was collected for 10 mins prior to calibration to ensure a stable signal. After 10 min of
789 imaging 50 µM TPA was added to the dish to collect the minimum FRET ratio of the sensor.
790 Once a stable signal had been achieved cells were then washed with phosphate, calcium, and
791 magnesium-free HEPES-buffered HBSS, pH = 7.4 to remove the chelate and then treated with
792 pyrithione and Zn with 0.001% (w/v) saponin.

793 All imaging data were analyzed in MATLAB (Mathworks). Images were background
794 corrected by subtracting a local background intensity from each pixel grouped in a certain
795 region of the image. Regions of interest were generated by using a segmentation algorithm
796 that segments the image based on the fluorescence intensity of the FRET ratio channel to
797 obtain single cell traces. FRET ratios for each cell trace were calculated by dividing the
798 background-corrected YFP FRET intensity by the background-corrected CFP intensity. The

bioRxiv preprint doi: https://doi.org/10.1101/2021.03.18.436026; this version posted March 18, 2021. The copyright holder for this preprint (which was not certified by peer review) is the author/funder, who has granted bioRxiv a license to display the preprint in perpetuity. It is made available under aCC-BY 4.0 International license.

resting, minimum, and maximum FRET ratios for each cell were used to calculate the fractional saturation, the dynamic range, and the reported [Zn] from the sensor in each cell. Resting [Zn] is calculated by $[Zn^{2+}] = K_d * (\frac{R_{Resting} - R_{min}}{R_{max} - R_{Resting}})^{1/hill}$ where the K_d = 230 pM and hill = 0.53 for NES-ZapCV2. The dynamic range of the sensor can be impacted by both over expression and under expression of the sensor which has a negative impact on the fidelity of the apparent [Zn]. For this reason, cells were excluded from the analysis if they fell outside of an acceptable dynamic range, 1.6 – 2.3 for the NES-ZapCV2 sensor.

Flow cytometry study of infection outcome with varied zinc availability

Four different media conditions were used for flow cytometry. Standard macrophage growth media (DMEM + 20% FBS) was found to contain 25 μM Zn by ICP-MS and was used as the baseline. The other three medias used chelex-100-treated FBS. Briefly, FBS was treated with Chelex 100 resin (Sigma-Aldrich, St. Louis, MO, USA) for 5 hours, stirring at 4 ˚C, followed by sterile filtration using a 0.22 μm PES membrane filter. This chelex-treated FBS was used to prepare the baseline Chelex media, which contained DMEM + 20% FBS + L-glutamine (2 mM) + sodium pyruvate (1 mM). Zn replete media was made by adding 30 μM $ZnCl_2$ (Sigma-Aldrich, St. Louis, MO, USA) to Chelex media. Media with essentially no Zn was made by adding 3 μM 2-{[Bis(2-pyridinylmethyl)amino]ethylamino}benzenesulfonic (ZX1, an extracellular Zn chelator(61)) (Strem Chemicals, Inc.) to Chelex media. ICP-MS measurements were carried out as described previously(62) to quantify the metal content of the media. While Chelex treatment depleted Zn, Ca, and Fe, the Zn replete, Chelexed media, and Zn deficient media are identical except for the amount of zinc present in the media (34 μM, 4 μM, no Zn, respectively).

bioRxiv preprint doi: https://doi.org/10.1101/2021.03.18.436026; this version posted March 18, 2021. The copyright holder for this preprint (which was not certified by peer review) is the author/funder, who has granted bioRxiv a license to display the preprint in perpetuity. It is made available under aCC-BY 4.0 International license.

For analysis of intracellular bacterial replication, monocytes from three mice were grown and differentiated to macrophages in 6 well plates. Six days later, *Salmonella* expressing pDiGc and induced with arabinose were grown to stationary phase with aeration. Macrophages were infected with *Salmonella* at a multiplicity of infection of 30, and infection proceeded for 45 min. At this point *Salmonella* media was removed, cells were washed 3x in PBS, and initial inoculum cells were collected by scraping with a nylon cell lifter (Corning™ C3008) and homogenized by pipetting gently with a P1000. Homogenized cells were fixed in a gentle fixative for preserving fluorescent protein fluorescence (1 % PFA and 1 % sucrose) for 15 min and then washed and resuspended in PBS and chilled at 4 ˚C. Media in all other samples was changed to experimental conditions which included 10 μg/mL gentamicin. Three wells were treated with each media, for each time point. At 2, 10, 18 and 24 Hrs post infection, cells were rinsed, lifted, fixed and chilled as above. Samples were analyzed on a BD FACSCelesta™ (BD Bioscences) collecting forward scatter area and width, side scatter area and width, 488 nm excitation 530/30 nm emission, and 561 nm excitation and 585/15 nm emission. Data were analyzed using FlowJo 10.5.3 software (FlowJo LLC).

The cell gating hierarchy was set as Single cells > GFP positive cells > Cells containing replicated bacteria. 25-30,000 single cells were collected per sample. Single cells were determined first by forward scatter area versus side scatter area then by side scatter width versus side scatter area. Non-fluorescent uninfected cells were used to set the gate for GFP positive cells. A ratio of the 488 nm channel to the 561 nm channel was taken by dividing 488 nm intensity by 561 nm intensity. Samples collected at 2 Hrs post infection were used as the "initial inoculum" to determine the fluorescence intensities for cells infected with bacteria that

bioRxiv preprint doi: https://doi.org/10.1101/2021.03.18.436026; this version posted March 18, 2021. The copyright holder for this preprint (which was not certified by peer review) is the author/funder, who has granted bioRxiv a license to display the preprint in perpetuity. It is made available under aCC-BY 4.0 International license.

have not undergone replication. Cells containing replicated bacteria were gated as having a 488 nm:561 nm ratio above the initial inoculum.

Acknowledgements

We would like to thank Dr. Lynn Sanford for technical assistance developing code for analyzing RNAseq data. We acknowledge the BioFrontiers Institute Advanced Light Microscopy Core, where spinning disc confocal microscopy was performed on a Nikon Ti-E microscope supported by the BioFrontiers Institute and the Howard Hughes Medical Institute. We would like to acknowledge the University of Colorado BioFrontiers Institute Next-Gen Sequencing Core Facility, which performed the Illumina sequencing and library construction, the BioFrontiers high-performance computing resources (NIH 1S10OD012300) supported by BioFrontiers' IT, and the University of Colorado Biochemistry Cell Culture Core Facility for providing resources and support in culturing.

Data availability

All raw next-generation sequencing data files and processed data files used to draw conclusions are available at the Gene Expression Omnibus, data series GSE166642.

Figure captions

Figure 1: Salmonella treatment of macrophages induces global RNA expression changes across two primary axes: time post exposure and *Salmonella* status (live vs. heat killed)

bioRxiv preprint doi: https://doi.org/10.1101/2021.03.18.436026; this version posted March 18, 2021. The copyright holder for this preprint (which was not certified by peer review) is the author/funder, who has granted bioRxiv a license to display the preprint in perpetuity. It is made available under aCC-BY 4.0 International license.

A) Schematic of infection experimental design for 129S6 BMDMs exposed to live or heat killed *Salmonella* Typhimurium SL1344. B) Global principal component analysis (PCA) with x-axis showing differential expression correlated with time post exposure and y-axis showing differential expression correlated with *Salmonella* status (live, heat killed (HK) or unexposed (UE)).

Figure 2: Clustered data exposes multiple distinct expression trends in global data

Four of the twenty groups that emerged from clustering analysis are presented as a box and whisker plot of gene expression levels as Z-scores (normalized across all DE genes) and a hierarchically clustered heat map of gene expression as rlog-scaled DESeq2 normalized counts. A) Group 1 contains 1462 genes that increase in expression at 2 Hrs and increase further at 18 Hrs, without significant differences between the Alive and HK conditions. B) Group 2 contains 1141 genes that increase in expression at 2 Hrs and then decrease below baseline at 18 Hrs. C) Group 8 contains 1028 genes which are expressed in unexposed cells, but then decrease as a function of time post infection. D) Group 10 contains 1480 genes that decrease in expression at 2 Hrs and increase at 18 Hrs. UE: unexposed control cells; HK: stimulation with heat killed bacteria.

Figure 3: GSEA reveals enrichment of the hypoxia and complement Hallmark gene sets in BMDMs infected with live *Salmonella* compared to treatment with heat killed bacteria.

Each panel shows a GSEA enrichment plot for a Hallmark gene set and a hierarchically clustered expression heat map of the leading edge genes from that GSEA plot. In GSEA plots each gene is

bioRxiv preprint doi: https://doi.org/10.1101/2021.03.18.436026; this version posted March 18, 2021. The copyright holder for this preprint (which was not certified by peer review) is the author/funder, who has granted bioRxiv a license to display the preprint in perpetuity. It is made available under aCC-BY 4.0 International license.

represented by a vertical black line, and leading edge genes are on the positive end of the spectrum, up to the point of maximum Enrichment Score. **A)** GSEA and heat map of leading edge genes for the Hallmark hypoxia gene set enriched in the 2 Hr Alive condition compared to 2 Hr HK (q = 0.000, NES = 2.12). **B)** GSEA and heat map of leading edge genes for the Hallmark hypoxia gene set enriched in the 18 Hr Alive condition compared to 18 Hr HK. At 18 Hrs, analysis of the hypoxia gene set shows 50 leading edge genes vs. 36 at 2 Hrs. Only 20 of these genes are in the leading edge at both time points. (q = 0.024, NES = 1.65). **C)** GSEA and heat map of leading edge genes for the Hallmark complement gene set enriched in the 2 Hr Alive condition vs. 2 Hr HK (q = 0.062, NES = 1.44). **D)** GSEA and heat map of leading edge genes for the Hallmark complement gene set enriched in the 18 Hr Alive condition vs. 18 Hr HK (q = 0.042, NES = 1.57). 42 complement genes appear in the leading edge, compared to 36 at 2 Hrs. While there is a core set of 16 genes upregulated at both time points, the remaining genes are unique. UE: unexposed control; HK: heat killed; q: false discovery rate; NES: Normalized Enrichment Score from GSEA.

Figure 4: GSEA reveals enrichment of the apoptosis Hallmark gene set at 2 Hrs and the UPR gene set at 18 Hrs in BMDMs treated with live versus heat killed *Salmonella*.

A) GSEA curve of the Hallmark apoptosis gene set, showing enrichment in the 2 Hr alive condition vs. the 2 Hr HK condition (q = 0.023, NES = 1.58). **B)** Heatmap of 25 leading edge apoptosis genes. **C)** GSEA curve of the Hallmark UPR gene set, showing enrichment in the 18 Hr Alive condition vs. the 18 Hr HK condition (q = 0.021, NES = 1.69). **D)** Heatmap of the 47 leading

bioRxiv preprint doi: https://doi.org/10.1101/2021.03.18.436026; this version posted March 18, 2021. The copyright holder for this preprint (which was not certified by peer review) is the author/funder, who has granted bioRxiv a license to display the preprint in perpetuity. It is made available under aCC-BY 4.0 International license.

907 edge UPR genes. UE: unexposed control; HK: heat killed; q: false discovery rate; NES:
908 Normalized Enrichment Score from GSEA.
909
910 **Figure 5: There are widespread changes in metal-transport, -dependent and homeostasis**
911 **genes.**
912 **A)** Schematic of major metal ion transporters and buffering proteins in macrophages. Slc30a1-
913 10 are also referred to as ZnT1-10. Slc39a1-14 are also referred to as Zip1-14. **B-D)** Heatmaps
914 of subsets of metal-transport, -dependent, and -homeostasis genes that are highly expressed
915 and differentially expressed in our data set (log ratio test $q < 0.01$, mean normalized counts >
916 100). These gene sets are curated to focus on nutritional immunity metals, including Fe, Zn, Cu,
917 and Mn. Genes that fit in multiple categories are only listed once. **B)** Metal ion transporters. **C)**
918 Metal-dependent and -responsive genes. **D)** Metal ion homeostasis genes. UE: unexposed
919 control cells; HK: heat killed bacteria exposure.
920
921 **Figure 6: Changes in labile cytosolic Zn in 129S6 BMDMs upon infection with *Salmonella***
922 A) Representative image of BMDMs expressing the NES-ZapCV2 fluorescent Zn sensor (green)
923 treated with *Salmonella* constitutively expressing mCherry (red). Scale bar = 20 μm. B)
924 Representative *in situ* calibration of the NES-ZapCV2 sensor showing the FRET ratio (R,
925 background corrected FRET channel divided by the background corrected CFP channel) over
926 time. The R_{min} is obtained upon addition of 50μM TPA and the R_{max} is obtained upon addition of
927 23.8nM buffered Zn, 0.001% saponin and 0.75μM pyrithione. Each trace represents a single
928 cell. C) Fractional saturation of the NES-ZapCV2 sensor at different time points post infection.

bioRxiv preprint doi: https://doi.org/10.1101/2021.03.18.436026; this version posted March 18, 2021. The copyright holder for this preprint (which was not certified by peer review) is the author/funder, who has granted bioRxiv a license to display the preprint in perpetuity. It is made available under aCC-BY 4.0 International license.

929 Each dot represents an individual cell. Data represent at least two independent experiments
930 per time point.
931
932 **Figure 7: Bacterial clearance as a function of time and Zn availability**
933 **A)** Schematic of the experimental protocol. Salmonella expressing the pDiGc plasmid expresses
934 GFP constitutively and DSRed under arabinose induction. Bacteria are cultured with arabinose
935 and aeration to the stationary phase, at which point they express both fluorescent proteins.
936 Arabinose is removed at infection, and infected macrophages are fluorescent in both red and
937 green channels by flow cytometry. As infection proceeds the green to red fluorescent ratio
938 'tracks' the bacteria. **B)** Metal content of normal growth media and media containing Chelex-
939 treated FBS, as determined by inductively coupled plasma mass spectrometry (ICP-MS). **C)**
940 Histograms of the GFP signal in macrophages expressing pDiGc in 4 different medias and at 4
941 time points. Each experimental condition was done in triplicate, and 10,000 cells were
942 measured per sample. Replicates were essentially identical, so data for the replicates was
943 concatenated. Increasing color saturation indicates time post *Salmonella* exposure (2, 10, 18 or
944 24 hours). The right peak in each graph corresponds to the GFP+ macrophages, indicating
945 infection. As *Salmonella* are cleared the macrophages become GFP- and shift to the left peak on
946 each graph. At the initial inoculation (white curve in each panel), macrophages show almost
947 100% infection rate. Normal macrophage growth media and Chelexed media supplemented
948 with 30 µM Zn (replete Zn conditions) show almost 100% bacterial clearance at 24 hours.
949 Chelexed media (low Zn) shows decreased bacterial clearance while Chelexed media with 3 µM
950 extracellular zinc chelator ZX1, (essentially no Zn) shows poor bacterial clearance.

bioRxiv preprint doi: https://doi.org/10.1101/2021.03.18.436026; this version posted March 18, 2021. The copyright holder for this preprint (which was not certified by peer review) is the author/funder, who has granted bioRxiv a license to display the preprint in perpetuity. It is made available under aCC-BY 4.0 International license.

Figure 8: Bacterial replication as a function of time and Zn availability

129S6 BMDMs were infected with *Salmonella* expressing pDiGc. The GFP and DsRed signals in BMDMs were measured by flow cytometry and plotted against one another. These density graphs show only macrophages containing GFP^+ *Salmonella*, which indicates active infection. Percentages on each plot indicate the number of macrophages with diluted DSRed signal, an indicator of *Salmonella* division. Dilution of DsRed is a function of time and zinc availability, with all media conditions showing an increase in bacterial division over time, but control and zinc replete conditions (first and second rows) show much more robust division.

Figure 9: Changes in metal-transport and -homeostasis genes reveal differences in metal regulation in BMDMs derived from Slc11a1-functional mice compared to nonfunctional mice.

RNAseq data from this study are compared to data from Stapels et al, GEO Accession GSE104785. Data from both studies were processed through the same pipeline and normalized together. Gene lists were compiled using Uniprot keywords and the mouse genome, and filtered for mean normalized count > 5 in at least one data set. A) Genes involved in Fe transport and homeostasis. B) Genes involved in Cu transport and homeostasis. C) Genes involved in Zn transport and homeostasis. UE: 129S6 BMDMs unexposed to *Salmonella*; HK: heat killed *Salmonella* treatment; UI: uninfected C57BL/6 BMDMs; G: C57BL/6 BMDMs containing growing *Salmonella*; BY: bystander C57BL/6 BMDMs.

bioRxiv preprint doi: https://doi.org/10.1101/2021.03.18.436026; this version posted March 18, 2021. The copyright holder for this preprint (which was not certified by peer review) is the author/funder, who has granted bioRxiv a license to display the preprint in perpetuity. It is made available under aCC-BY 4.0 International license.

973 **REFERENCES**

974 1. Hood MI, Skaar EP. Nutritional immunity: transition metals at the pathogen–host
975 interface. Nat Rev Microbiol. 2012 Aug;10(8):525–37.

976 2. Kehl-Fie TE, Skaar EP. Nutritional immunity beyond iron: a role for manganese and zinc.
977 Curr Opin Chem Biol. 2010 Apr;14(2):218–24.

978 3. Ganz T. Iron and infection. Int J Hematol. 2018 Jan;107(1):7–15.

979 4. White C, Lee J, Kambe T, Fritsche K, Petris MJ. A Role for the ATP7A Copper-transporting
980 ATPase in Macrophage Bactericidal Activity*. J Biol Chem. 2009 Dec 4;284(49):33949–56.

981 5. Djoko KY, Ong CY, Walker MJ, McEwan AG. The Role of Copper and Zinc Toxicity in Innate
982 Immune Defense against Bacterial Pathogens *. J Biol Chem. 2015 Jul 31;290(31):18954–
983 61.

984 6. Cassat JE, Skaar EP. Iron in Infection and Immunity. Cell Host Microbe. 2013 May
985 15;13(5):509–19.

986 7. Gao H, Dai W, Zhao L, Min J, Wang F. The Role of Zinc and Zinc Homeostasis in
987 Macrophage Function. J Immunol Res [Internet]. 2018 Dec 6 [cited 2021 Jan 25];2018.
988 Available from: https://www.ncbi.nlm.nih.gov/pmc/articles/PMC6304900/

989 8. Andreini C, Bertini I. A bioinformatics view of zinc enzymes. J Inorg Biochem. 2012 Jun
990 1;111:150–6.

991 9. Vinkenborg JL, Nicolson TJ, Bellomo EA, Koay MS, Rutter GA, Merkx M. Genetically
992 encoded FRET sensors to monitor intracellular Zn2+ homeostasis. Nat Methods. 2009
993 Oct;6(10):737–40.

994 10. Qin Y, Miranda JG, Stoddard CI, Dean KM, Galati DF, Palmer AE. Direct Comparison of a
995 Genetically Encoded Sensor and Small Molecule Indicator: Implications for Quantification
996 of Cytosolic Zn2+. ACS Chem Biol. 2013 Nov 15;8(11):2366–71.

997 11. Qin Y, Dittmer PJ, Park JG, Jansen KB, Palmer AE. Measuring steady-state and dynamic
998 endoplasmic reticulum and Golgi Zn2+ with genetically encoded sensors. Proc Natl Acad
999 Sci. 2011 May 3;108(18):7351–6.

1000 12. Chabosseau P, Tuncay E, Meur G, Bellomo EA, Hessels A, Hughes S, et al. Mitochondrial
1001 and ER-Targeted eCALWY Probes Reveal High Levels of Free Zn2+. ACS Chem Biol. 2014
1002 Sep 19;9(9):2111–20.

1003 13. Park JG, Palmer AE. Quantitative Measurement of Ca2+ and Zn2+ in Mammalian Cells
1004 Using Genetically Encoded Fluorescent Biosensors. In: Zhang J, Ni Q, Newman RH, editors.
1005 Fluorescent Protein-Based Biosensors: Methods and Protocols [Internet]. Totowa, NJ:

bioRxiv preprint doi: https://doi.org/10.1101/2021.03.18.436026; this version posted March 18, 2021. The copyright holder for this preprint (which was not certified by peer review) is the author/funder, who has granted bioRxiv a license to display the preprint in perpetuity. It is made available under aCC-BY 4.0 International license.

Humana Press; 2014 [cited 2021 Mar 5]. p. 29–47. (Methods in Molecular Biology). Available from: https://doi.org/10.1007/978-1-62703-622-1_3

14. Carter KP, Carpenter MC, Fiedler B, Jimenez R, Palmer AE. Critical Comparison of FRET-Sensor Functionality in the Cytosol and Endoplasmic Reticulum and Implications for Quantification of Ions. Anal Chem. 2017 Sep 5;89(17):9601–8.

15. Pratt EPS, Damon LJ, Anson KJ, Palmer AE. Tools and techniques for illuminating the cell biology of zinc. Biochim Biophys Acta BBA - Mol Cell Res. 2021 Jan 1;1868(1):118865.

16. Eide DJ. Zinc transporters and the cellular trafficking of zinc. Biochim Biophys Acta BBA - Mol Cell Res. 2006 Jul 1;1763(7):711–22.

17. Andrews GK. Cellular zinc sensors: MTF-1 regulation of gene expression. In: Maret W, editor. Zinc Biochemistry, Physiology, and Homeostasis: Recent Insights and Current Trends [Internet]. Dordrecht: Springer Netherlands; 2001 [cited 2021 Jan 20]. p. 37–51. Available from: https://doi.org/10.1007/978-94-017-3728-9_3

18. Gaddy JA, Haley KP. Metalloregulation of Helicobacter pylori physiology and pathogenesis. Front Microbiol [Internet]. 2015 [cited 2021 Jan 25];6. Available from: https://www.frontiersin.org/articles/10.3389/fmicb.2015.00911/full

19. Botella H, Peyron P, Levillain F, Poincloux R, Poquet Y, Brandli I, et al. Mycobacterial P1-Type ATPases Mediate Resistance to Zinc Poisoning in Human Macrophages. Cell Host Microbe. 2011 Sep 15;10(3):248–59.

20. Stocks CJ, Phan M-D, Achard MES, Nhu NTK, Condon ND, Gawthorne JA, et al. Uropathogenic Escherichia coli employs both evasion and resistance to subvert innate immune-mediated zinc toxicity for dissemination. Proc Natl Acad Sci. 2019 Mar 26;116(13):6341–50.

21. Stafford SL, Bokil NJ, Achard MES, Kapetanovic R, Schembri MA, McEwan AG, et al. Metal ions in macrophage antimicrobial pathways: emerging roles for zinc and copper. Biosci Rep [Internet]. 2013 Jul 16 [cited 2021 Jan 25];33(e00049). Available from: https://doi.org/10.1042/BSR20130014

22. Vignesh KS, Figueroa JAL, Porollo A, Caruso JA, Jr GSD. Zinc Sequestration: Arming Phagocyte Defense against Fungal Attack. PLOS Pathog. 2013 Dec 26;9(12):e1003815.

23. Ammendola S, Pasquali P, Pistoia C, Petrucci P, Petrarca P, Rotilio G, et al. High-Affinity Zn2+ Uptake System ZnuABC Is Required for Bacterial Zinc Homeostasis in Intracellular Environments and Contributes to the Virulence of Salmonella enterica. Infect Immun. 2007 Dec 1;75(12):5867–76.

bioRxiv preprint doi: https://doi.org/10.1101/2021.03.18.436026; this version posted March 18, 2021. The copyright holder for this preprint (which was not certified by peer review) is the author/funder, who has granted bioRxiv a license to display the preprint in perpetuity. It is made available under aCC-BY 4.0 International license.

24. Petrarca P, Ammendola S, Pasquali P, Battistoni A. The Zur-Regulated ZinT Protein Is an Auxiliary Component of the High-Affinity ZnuABC Zinc Transporter That Facilitates Metal Recruitment during Severe Zinc Shortage. J Bacteriol. 2010 Mar 15;192(6):1553–64.

25. Huang K, Wang D, Frederiksen RF, Rensing C, Olsen JE, Fresno AH. Investigation of the Role of Genes Encoding Zinc Exporters zntA, zitB, and fieF during Salmonella Typhimurium Infection. Front Microbiol [Internet]. 2018 [cited 2021 Feb 28];8. Available from: https://www.frontiersin.org/articles/10.3389/fmicb.2017.02656/full

26. Wu A, Tymoszuk P, Haschka D, Heeke S, Dichtl S, Petzer V, et al. Salmonella Utilizes Zinc To Subvert Antimicrobial Host Defense of Macrophages via Modulation of NF-κB Signaling. Infect Immun [Internet]. 2017 Dec 1 [cited 2021 Jan 24];85(12). Available from: https://iai.asm.org/content/85/12/e00418-17

27. Kapetanovic R, Bokil NJ, Achard MES, Ong CY, Peters KM, Stocks CJ, et al. Salmonella employs multiple mechanisms to subvert the TLR-inducible zinc-mediated antimicrobial response of human macrophages. FASEB J. 2016;30(5):1901–12.

28. Campoy S, Jara M, Busquets N, Rozas AMP de, Badiola I, Barbé J. Role of the High-Affinity Zinc Uptake znuABC System in Salmonella enterica Serovar Typhimurium Virulence. Infect Immun. 2002 Aug 1;70(8):4721–5.

29. Vidal SM, Pinner E, Lepage P, Gauthier S, Gros P. Natural resistance to intracellular infections: Nramp1 encodes a membrane phosphoglycoprotein absent in macrophages from susceptible (Nramp1 D169) mouse strains. J Immunol. 1996 Oct 15;157(8):3559–68.

30. Brown DE, Libby SJ, Moreland SM, McCoy MW, Brabb T, Stepanek A, et al. Salmonella enterica causes more severe inflammatory disease in C57/BL6 Nramp1G169 mice than Sv129S6 mice. Vet Pathol. 2013 Sep;50(5):867–76.

31. Saliba A-E, Li L, Westermann AJ, Appenzeller S, Stapels DAC, Schulte LN, et al. Single-cell RNA-seq ties macrophage polarization to growth rate of intracellular Salmonella. Nat Microbiol. 2017 Feb;2(2):16206.

32. Subramanian A, Tamayo P, Mootha VK, Mukherjee S, Ebert BL, Gillette MA, et al. Gene set enrichment analysis: A knowledge-based approach for interpreting genome-wide expression profiles. Proc Natl Acad Sci. 2005 Oct 25;102(43):15545–50.

33. Liberzon A, Birger C, Thorvaldsdóttir H, Ghandi M, Mesirov JP, Tamayo P. The Molecular Signatures Database Hallmark Gene Set Collection. Cell Syst. 2015 Dec 23;1(6):417–25.

34. Schaffer K, Taylor CT. The impact of hypoxia on bacterial infection. FEBS J. 2015;282(12):2260–6.

35. Wrande M, Vestö K, Puiac Banesaru S, Anwar N, Nordfjell J, Liu L, et al. Replication of Salmonella enterica serovar Typhimurium in RAW264.7 Phagocytes Correlates With

bioRxiv preprint doi: https://doi.org/10.1101/2021.03.18.436026; this version posted March 18, 2021. The copyright holder for this preprint (which was not certified by peer review) is the author/funder, who has granted bioRxiv a license to display the preprint in perpetuity. It is made available under aCC-BY 4.0 International license.

Hypoxia and Lack of iNOS Expression. Front Cell Infect Microbiol [Internet]. 2020 Nov 30 [cited 2021 Jan 25];10. Available from: https://www.ncbi.nlm.nih.gov/pmc/articles/PMC7734562/

36. Díaz-Bulnes P, Saiz ML, López-Larrea C, Rodríguez RM. Crosstalk Between Hypoxia and ER Stress Response: A Key Regulator of Macrophage Polarization. Front Immunol [Internet]. 2020 [cited 2021 Jan 27];10. Available from: https://www.frontiersin.org/articles/10.3389/fimmu.2019.02951/full

37. Bugla-Płoskońska G, Kiersnowski A, Futoma-Kołoch B, Doroszkiewicz W. Killing of Gram-Negative Bacteria with Normal Human Serum and Normal Bovine Serum: Use of Lysozyme and Complement Proteins in the Death of Salmonella Strains O48. Microb Ecol. 2009 Aug 1;58(2):276–89.

38. Dunkelberger JR, Song W-C. Complement and its role in innate and adaptive immune responses. Cell Res. 2010 Jan;20(1):34–50.

39. Monack DM, Raupach B, Hromockyj AE, Falkow S. Salmonella typhimurium invasion induces apoptosis in infected macrophages. Proc Natl Acad Sci. 1996 Sep 3;93(18):9833–8.

40. Pham CG, Bubici C, Zazzeroni F, Papa S, Jones J, Alvarez K, et al. Ferritin Heavy Chain Upregulation by NF-κB Inhibits TNFα-Induced Apoptosis by Suppressing Reactive Oxygen Species. Cell. 2004 Nov 12;119(4):529–42.

41. Dittmer PJ, Miranda JG, Gorski JA, Palmer AE. Genetically Encoded Sensors to Elucidate Spatial Distribution of Cellular Zinc. J Biol Chem. 2009 Jun 12;284(24):16289–97.

42. Kiedrowski L. Cytosolic zinc release and clearance in hippocampal neurons exposed to glutamate – the role of pH and sodium. J Neurochem. 2011;117(2):231–43.

43. Jeong J, Walker JM, Wang F, Park JG, Palmer AE, Giunta C, et al. Promotion of vesicular zinc efflux by ZIP13 and its implications for spondylocheiro dysplastic Ehlers–Danlos syndrome. Proc Natl Acad Sci. 2012 Dec 18;109(51):E3530–8.

44. Fiedler BL, Van Buskirk S, Carter KP, Qin Y, Carpenter MC, Palmer AE, et al. Droplet Microfluidic Flow Cytometer For Sorting On Transient Cellular Responses Of Genetically-Encoded Sensors. Anal Chem. 2017 Jan 3;89(1):711–9.

45. Sanford L, Palmer AE. Dissociated Hippocampal Neurons Exhibit Distinct Zn2+ Dynamics in a Stimulation-Method-Dependent Manner. ACS Chem Neurosci. 2020 Feb 19;11(4):508–14.

46. Helaine S, Cheverton AM, Watson KG, Faure LM, Matthews SA, Holden DW. Internalization of Salmonella by Macrophages Induces Formation of Nonreplicating Persisters. Science. 2014 Jan 10;343(6167):204–8.

bioRxiv preprint doi: https://doi.org/10.1101/2021.03.18.436026; this version posted March 18, 2021. The copyright holder for this preprint (which was not certified by peer review) is the author/funder, who has granted bioRxiv a license to display the preprint in perpetuity. It is made available under aCC-BY 4.0 International license.

47. Stapels DAC, Hill PWS, Westermann AJ, Fisher RA, Thurston TL, Saliba A-E, et al. Salmonella persisters undermine host immune defenses during antibiotic treatment. Science. 2018 Dec 7;362(6419):1156–60.

48. Liu M-J, Bao S, Gálvez-Peralta M, Pyle CJ, Rudawsky AC, Pavlovicz RE, et al. ZIP8 Regulates Host Defense through Zinc-Mediated Inhibition of NF-κB. Cell Rep. 2013 Feb 21;3(2):386–400.

49. Cunrath O, Bumann D. Host resistance factor SLC11A1 restricts Salmonella growth through magnesium deprivation. Science. 2019 Nov 22;366(6468):995–9.

50. Monack DM, Bouley DM, Falkow S. Salmonella typhimurium persists within macrophages in the mesenteric lymph nodes of chronically infected Nramp1+/+ mice and can be reactivated by IFNgamma neutralization. J Exp Med. 2004 Jan 19;199(2):231–41.

51. Núñez G, Sakamoto K, Soares MP. Innate Nutritional Immunity. J Immunol. 2018 Jul 1;201(1):11–8.

52. Subramanian Vignesh K, Landero Figueroa JA, Porollo A, Caruso JA, Deepe GS. Granulocyte Macrophage-Colony Stimulating Factor Induced Zn Sequestration Enhances Macrophage Superoxide and Limits Intracellular Pathogen Survival. Immunity. 2013 Oct 17;39(4):697–710.

53. Sayadi A, Nguyen A-T, Bard FA, Bard-Chapeau EA. Zip14 expression induced by lipopolysaccharides in macrophages attenuates inflammatory response. Inflamm Res. 2013 Feb 1;62(2):133–43.

54. Cerasi M, Liu JZ, Ammendola S, Poe AJ, Petrarca P, Pesciaroli M, et al. The ZupT transporter plays an important role in zinc homeostasis and contributes to Salmonella enterica virulence†. Metallomics. 2014 Apr 1;6(4):845–53.

55. Galván-Peña S, O'Neill LAJ. Metabolic Reprograming in Macrophage Polarization. Front Immunol [Internet]. 2014 [cited 2021 Jan 28];5. Available from: https://www.frontiersin.org/articles/10.3389/fimmu.2014.00420/full

56. Wemyss MA, Pearson JS. Host Cell Death Responses to Non-typhoidal Salmonella Infection. Front Immunol [Internet]. 2019 [cited 2021 Jan 27];10. Available from: https://www.frontiersin.org/articles/10.3389/fimmu.2019.01758/full

57. Orecchioni M, Ghosheh Y, Pramod AB, Ley K. Macrophage Polarization: Different Gene Signatures in M1(LPS+) vs. Classically and M2(LPS–) vs. Alternatively Activated Macrophages. Front Immunol [Internet]. 2019 [cited 2021 Feb 3];10. Available from: https://www.frontiersin.org/articles/10.3389/fimmu.2019.01084/full

bioRxiv preprint doi: https://doi.org/10.1101/2021.03.18.436026; this version posted March 18, 2021. The copyright holder for this preprint (which was not certified by peer review) is the author/funder, who has granted bioRxiv a license to display the preprint in perpetuity. It is made available under aCC-BY 4.0 International license.

58. Jablonski KA, Amici SA, Webb LM, Ruiz-Rosado J de D, Popovich PG, Partida-Sanchez S, et al. Novel Markers to Delineate Murine M1 and M2 Macrophages. Olszewski MA, editor. PLOS ONE. 2015 Dec 23;10(12):e0145342.

59. Eisele NA, Ruby T, Jacobson A, Manzanillo PS, Cox JS, Lam L, et al. Salmonella Require the Fatty Acid Regulator PPARδ for the Establishment of a Metabolic Environment Essential for Long-Term Persistence. Cell Host Microbe. 2013 Aug 14;14(2):171–82.

60. Subramanian A, Kuehn H, Gould J, Tamayo P, Mesirov JP. GSEA-P: a desktop application for Gene Set Enrichment Analysis. Bioinformatics. 2007 Dec 1;23(23):3251–3.

61. Pan E, Zhang X, Huang Z, Krezel A, Zhao M, Tinberg CE, et al. Vesicular Zinc Promotes Presynaptic and Inhibits Postsynaptic Long-Term Potentiation of Mossy Fiber-CA3 Synapse. Neuron. 2011 Sep 22;71(6):1116–26.

62. Carter KP. Engineering and Evaluating Fluorescent Tools for Endoplasmic Reticulum Zinc.

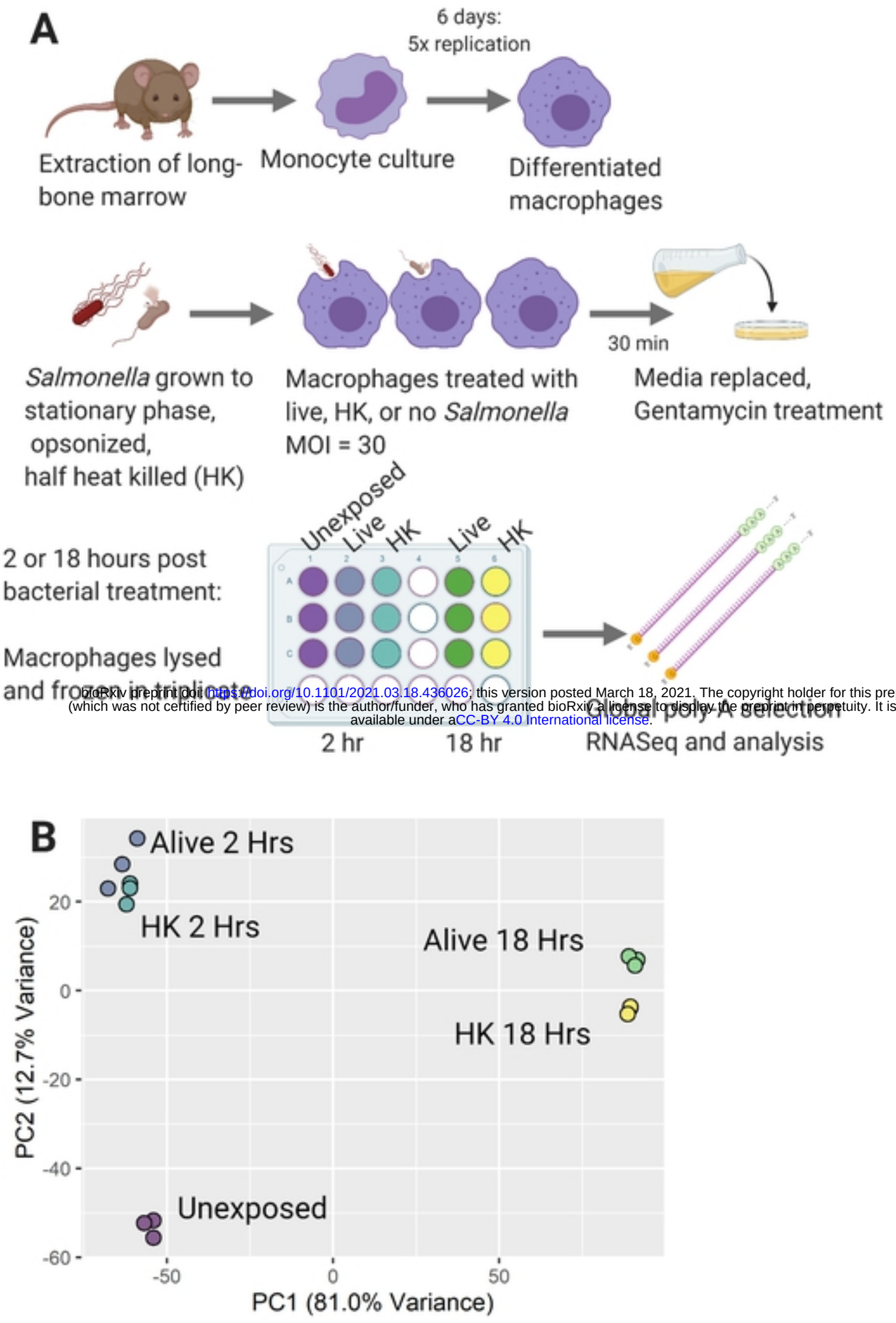

bioRxiv preprint doi: https://doi.org/10.1101/2021.03.18.436026; this version posted March 18, 2021. The copyright holder for this preprint (which was not certified by peer review) is the author/funder, who has granted bioRxiv a license to display the preprint in perpetuity. It is made available under aCC-BY 4.0 International license.

Figure 1

bioRxiv preprint doi: https://doi.org/10.1101/2021.03.18.436026; this version posted March 18, 2021. The copyright holder for this preprint (which was not certified by peer review) is the author/funder, who has granted bioRxiv a license to display the preprint in perpetuity. It is made available under aCC-BY 4.0 International license.

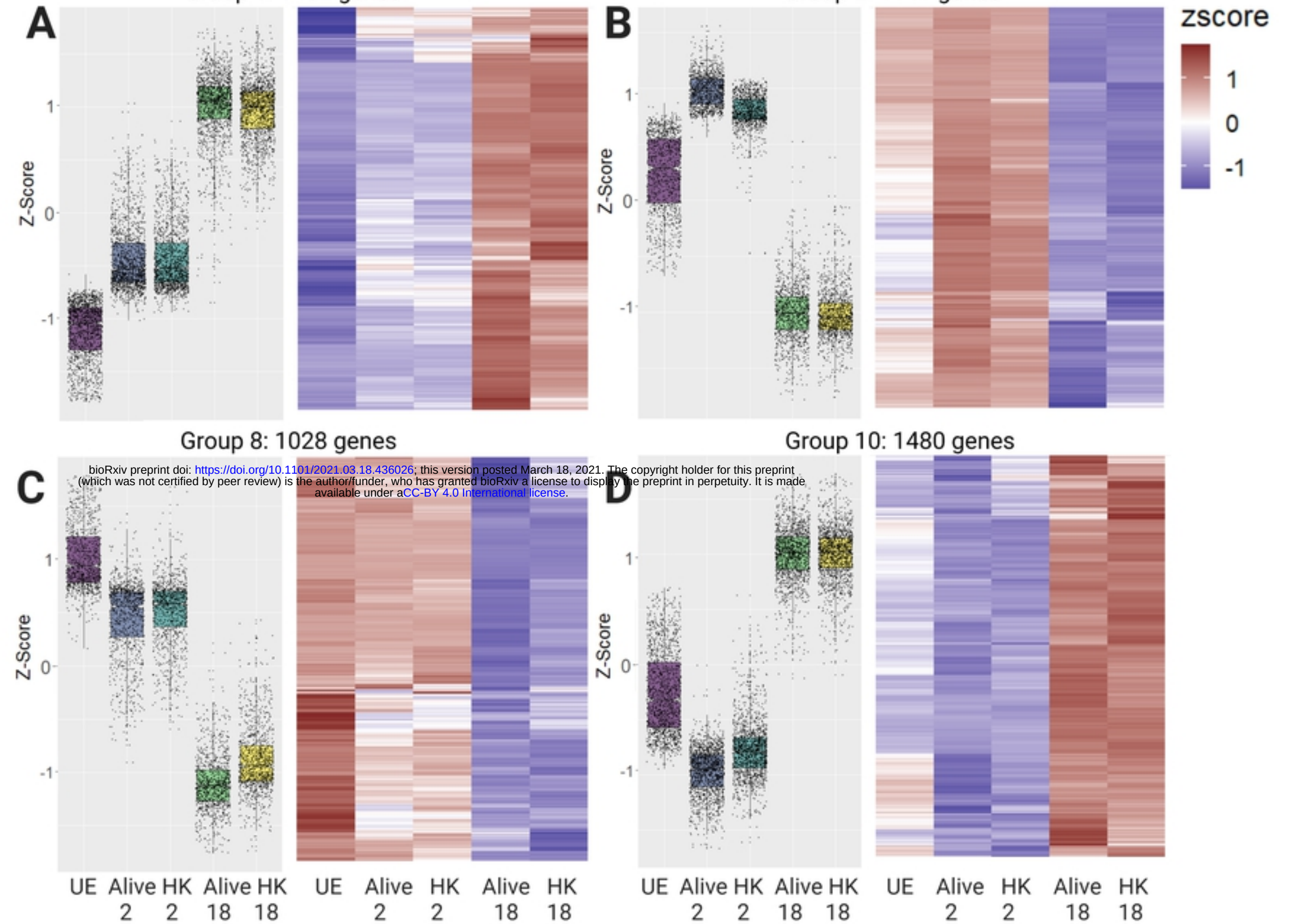

Figure 2

bioRxiv preprint doi: https://doi.org/10.1101/2021.03.18.436026; this version posted March 18, 2021. The copyright holder for this preprint (which was not certified by peer review) is the author/funder, who has granted bioRxiv a license to display the preprint in perpetuity. It is made available under aCC-BY 4.0 International license.

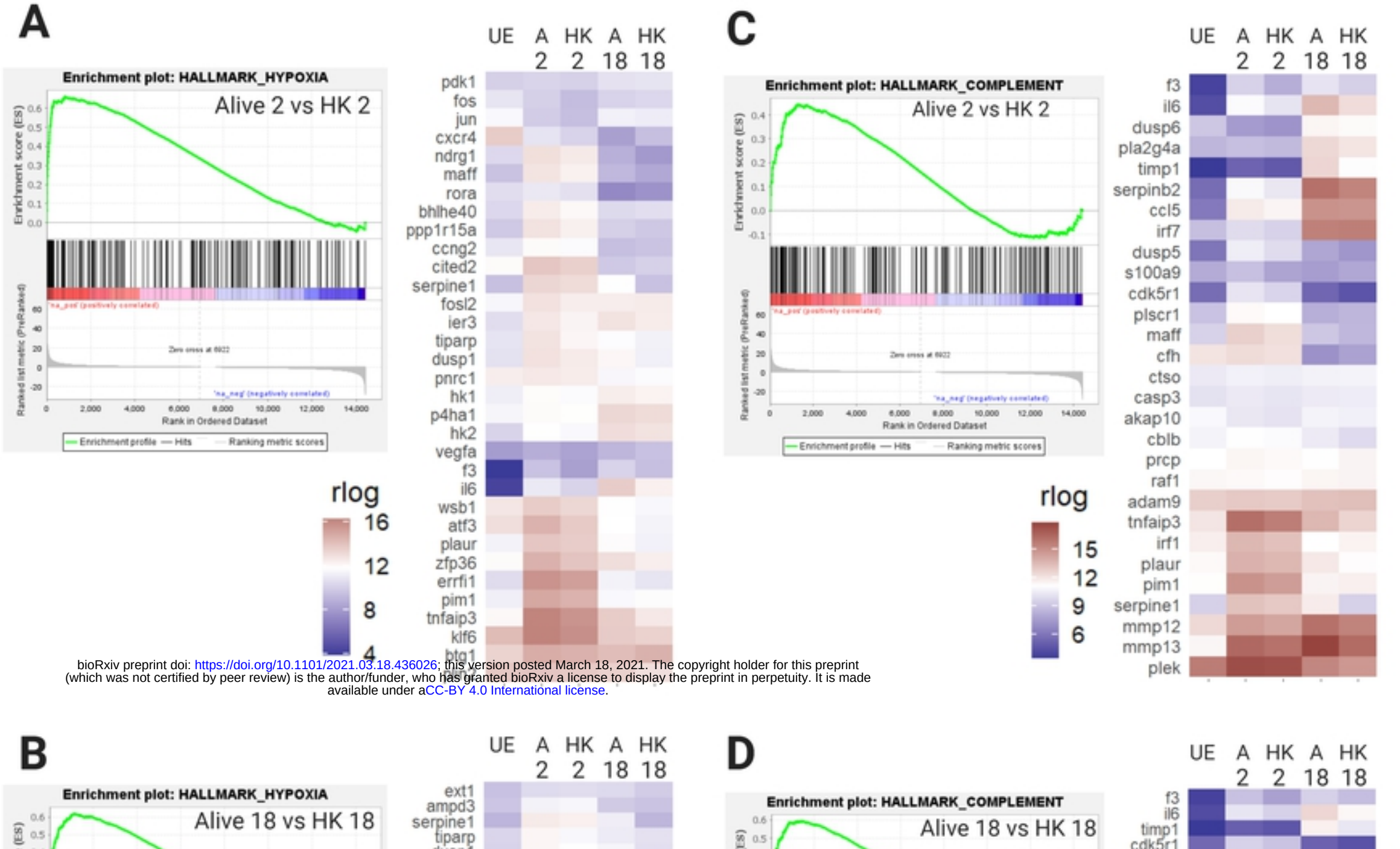

Figure 3

bioRxiv preprint doi: https://doi.org/10.1101/2021.03.18.436026; this version posted March 18, 2021. The copyright holder for this preprint (which was not certified by peer review) is the author/funder, who has granted bioRxiv a license to display the preprint in perpetuity. It is made available under aCC-BY 4.0 International license.

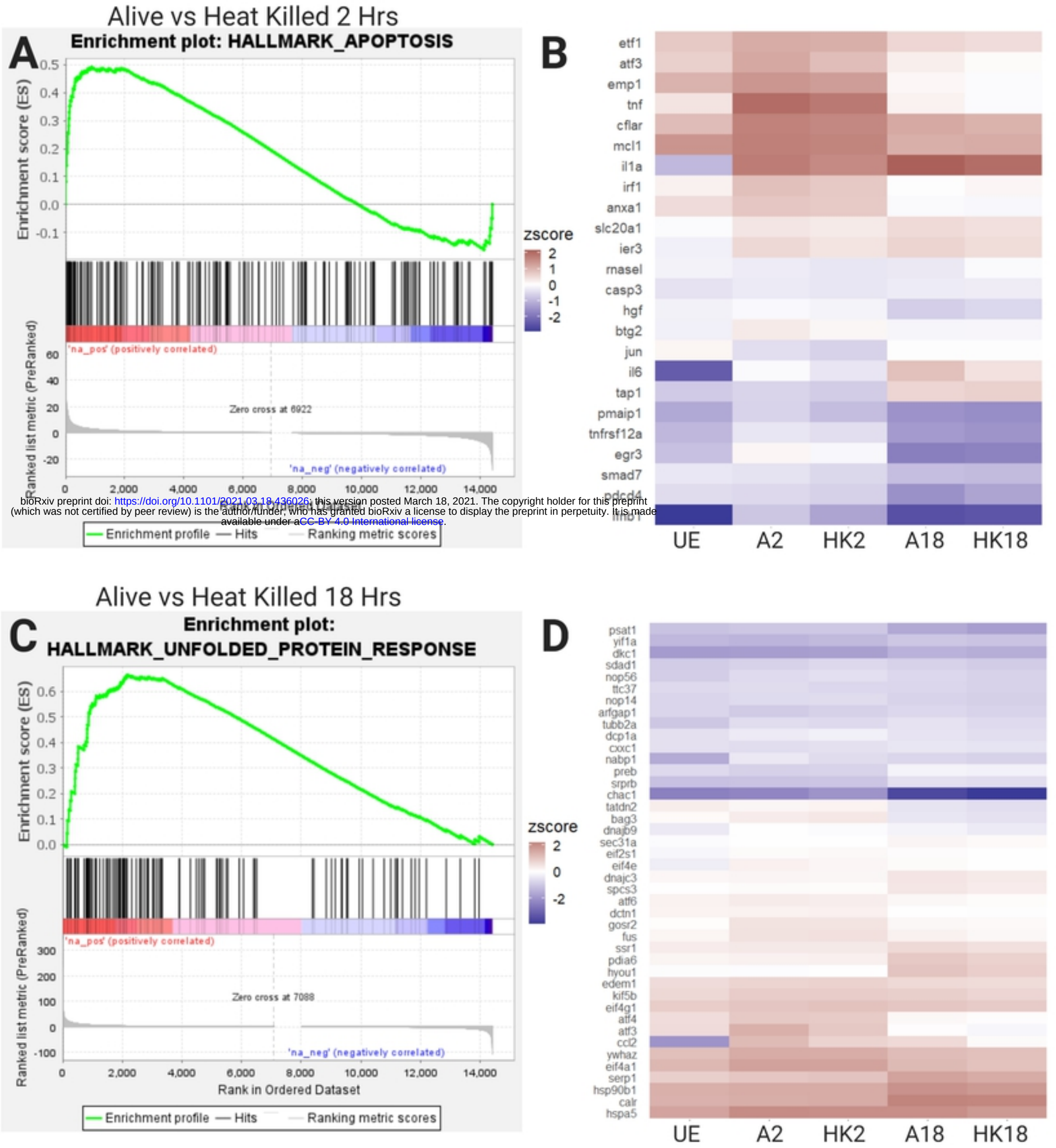

Figure 4

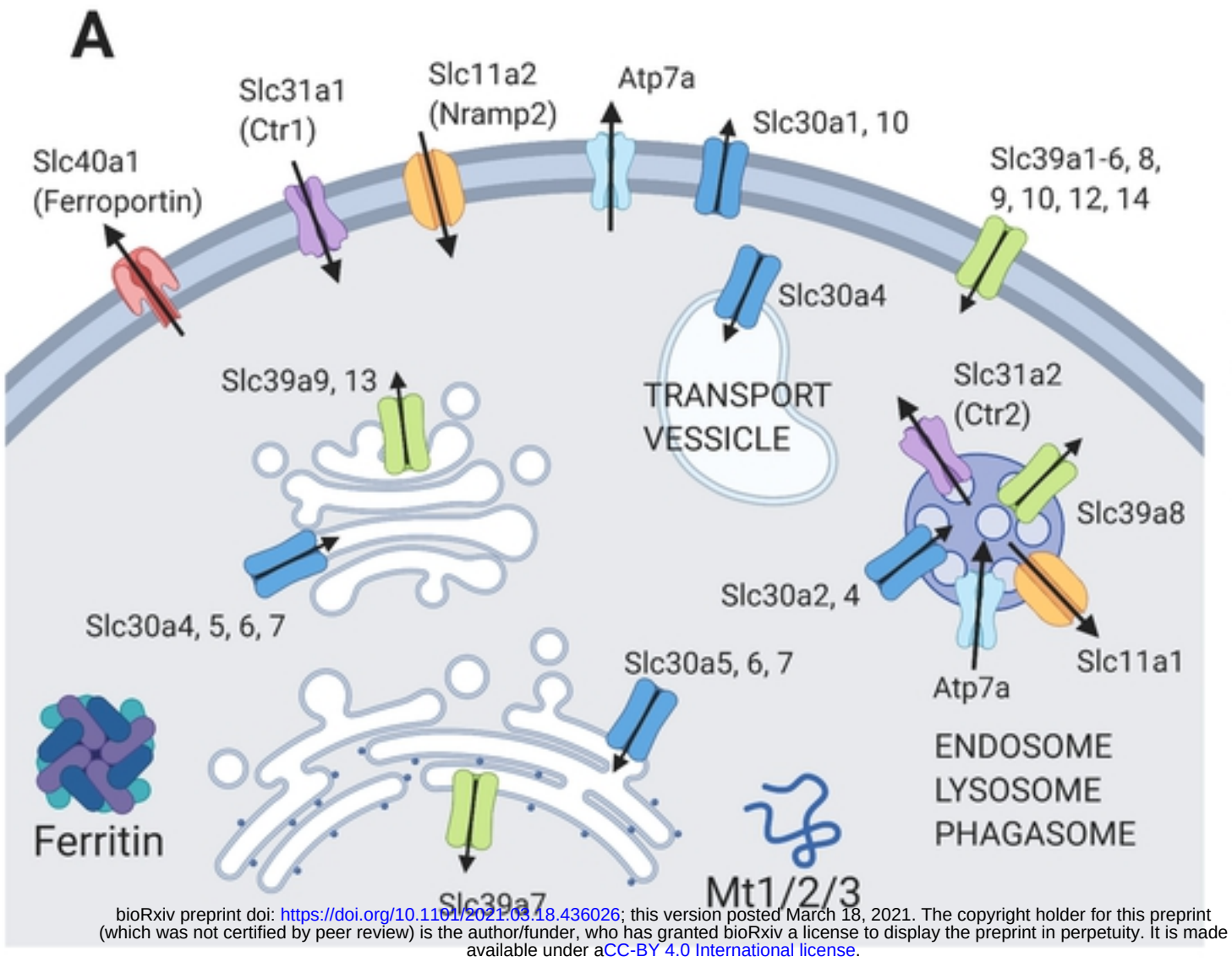

bioRxiv preprint doi: https://doi.org/10.1101/2021.03.18.436026; this version posted March 18, 2021. The copyright holder for this preprint (which was not certified by peer review) is the author/funder, who has granted bioRxiv a license to display the preprint in perpetuity. It is made available under aCC-BY 4.0 International license.

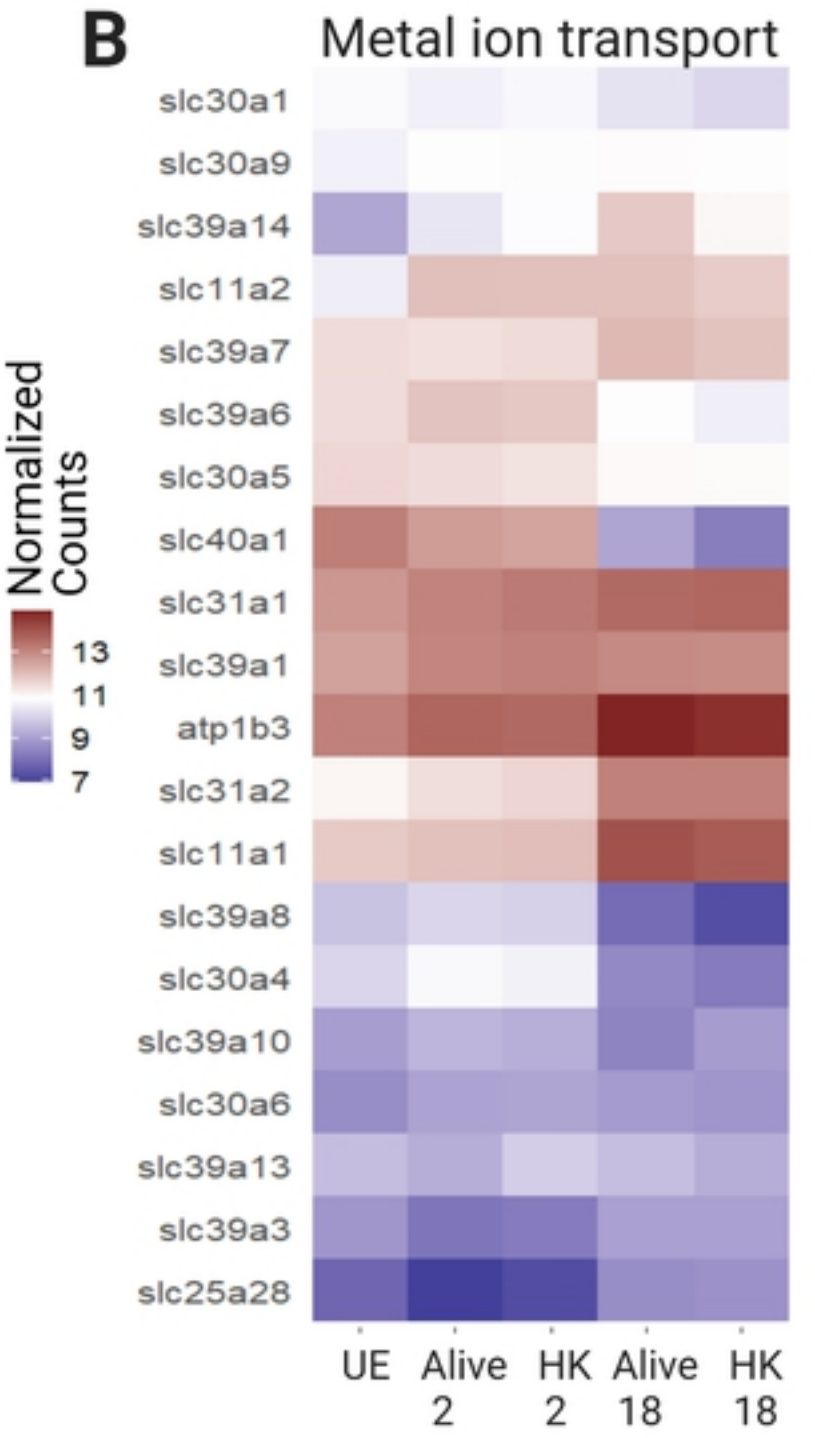

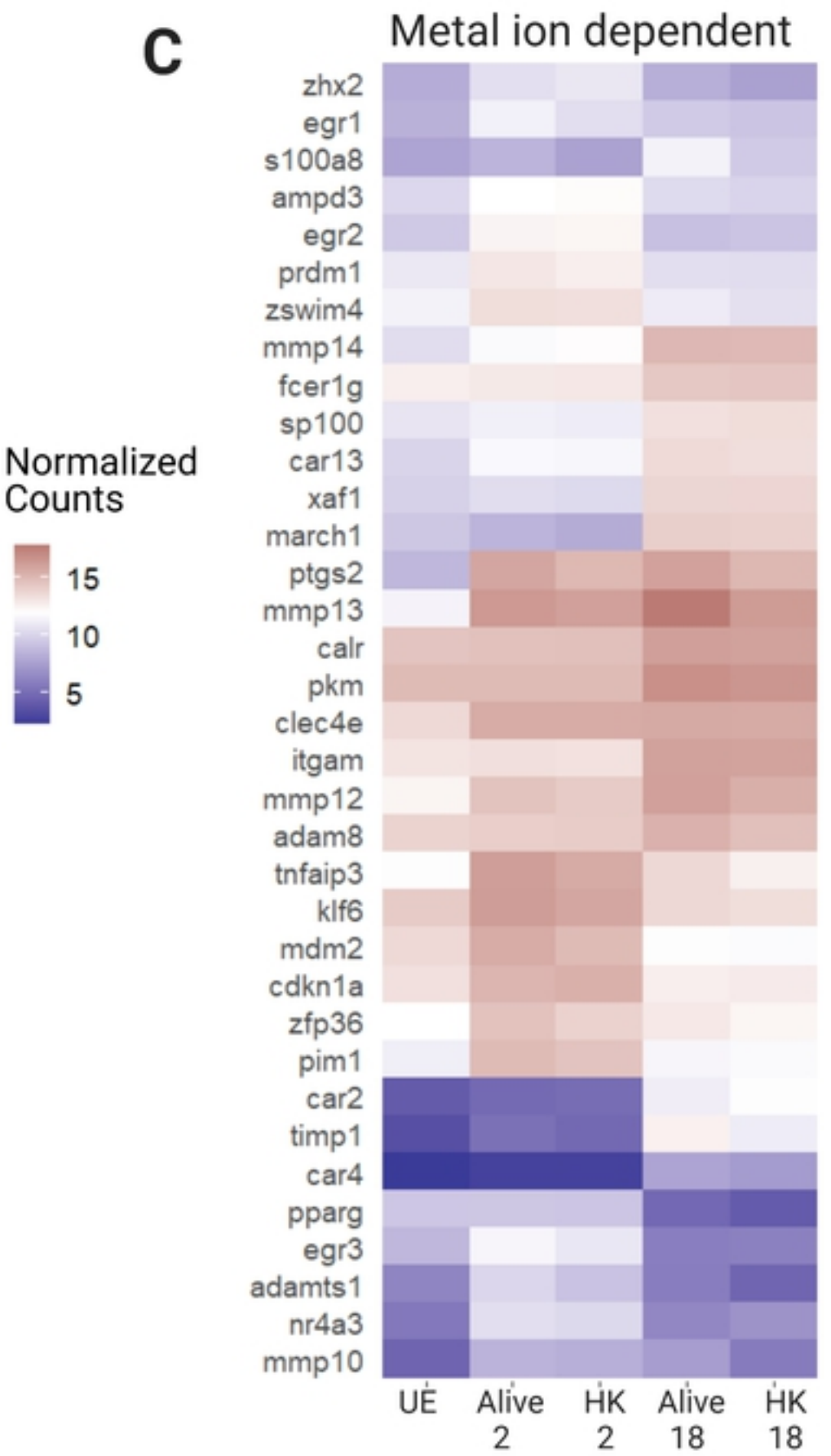

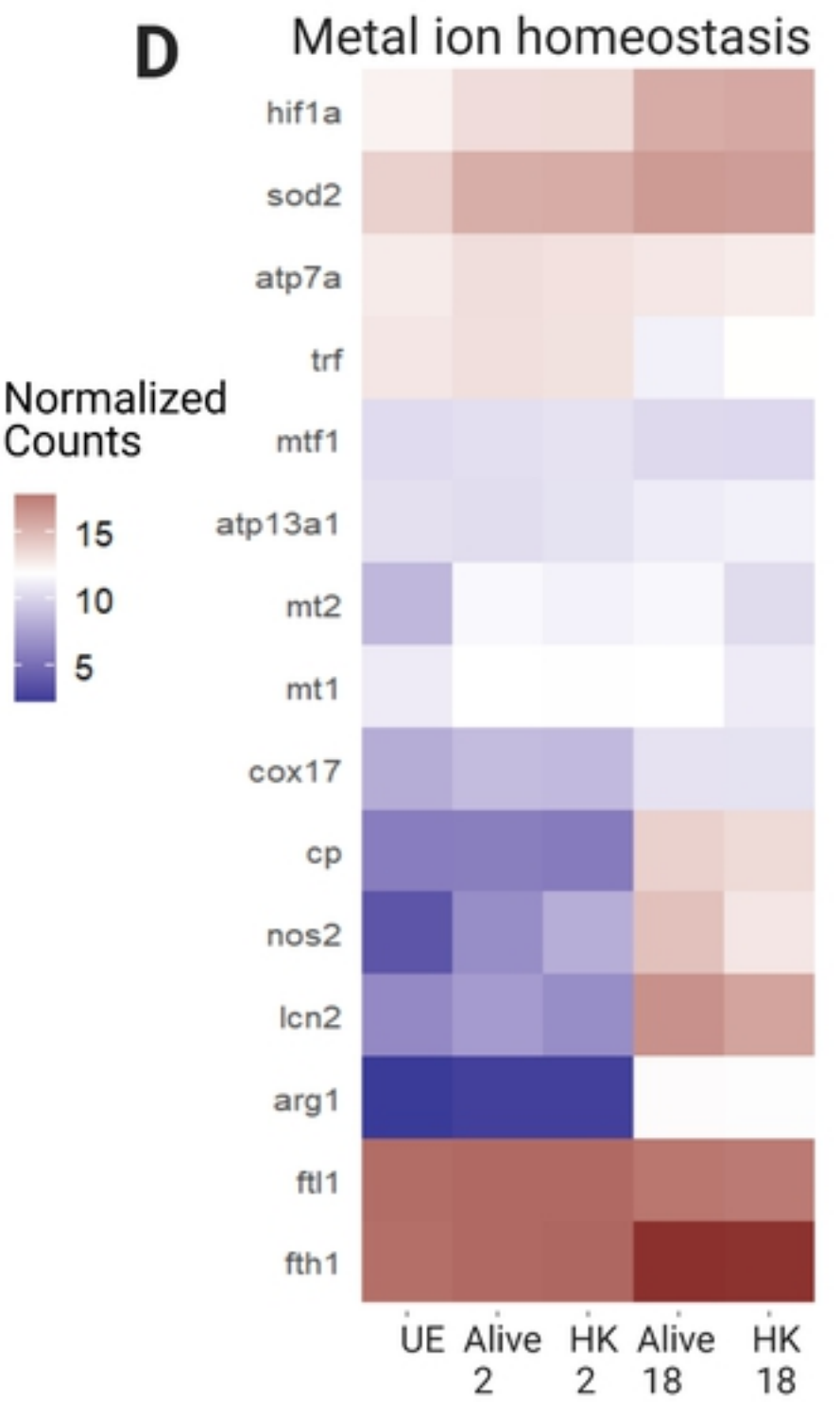

Figure 5

bioRxiv preprint doi: https://doi.org/10.1101/2021.03.18.436026; this version posted March 18, 2021. The copyright holder for this preprint (which was not certified by peer review) is the author/funder, who has granted bioRxiv a license to display the preprint in perpetuity. It is made available under aCC-BY 4.0 International license.

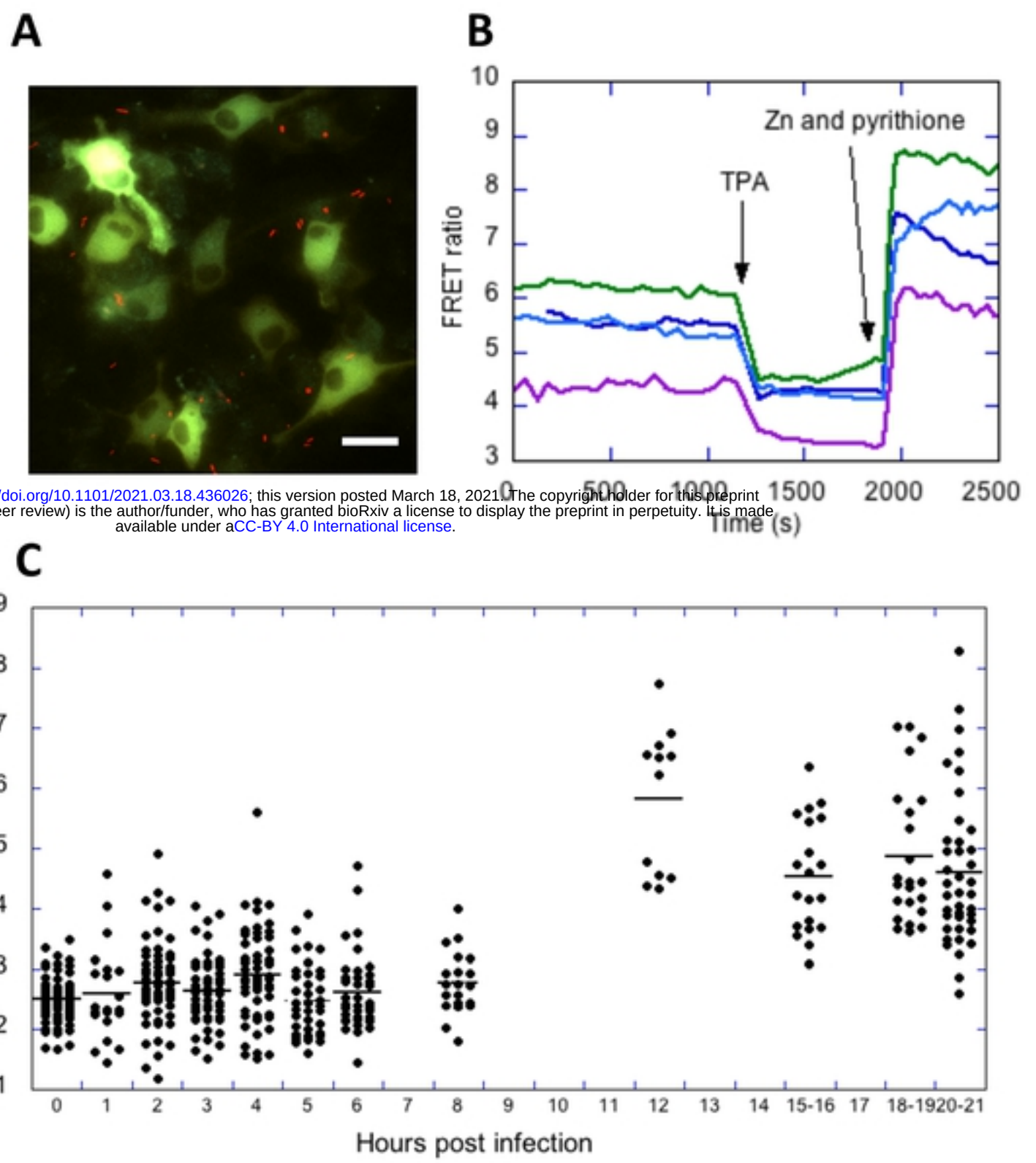

Figure 6

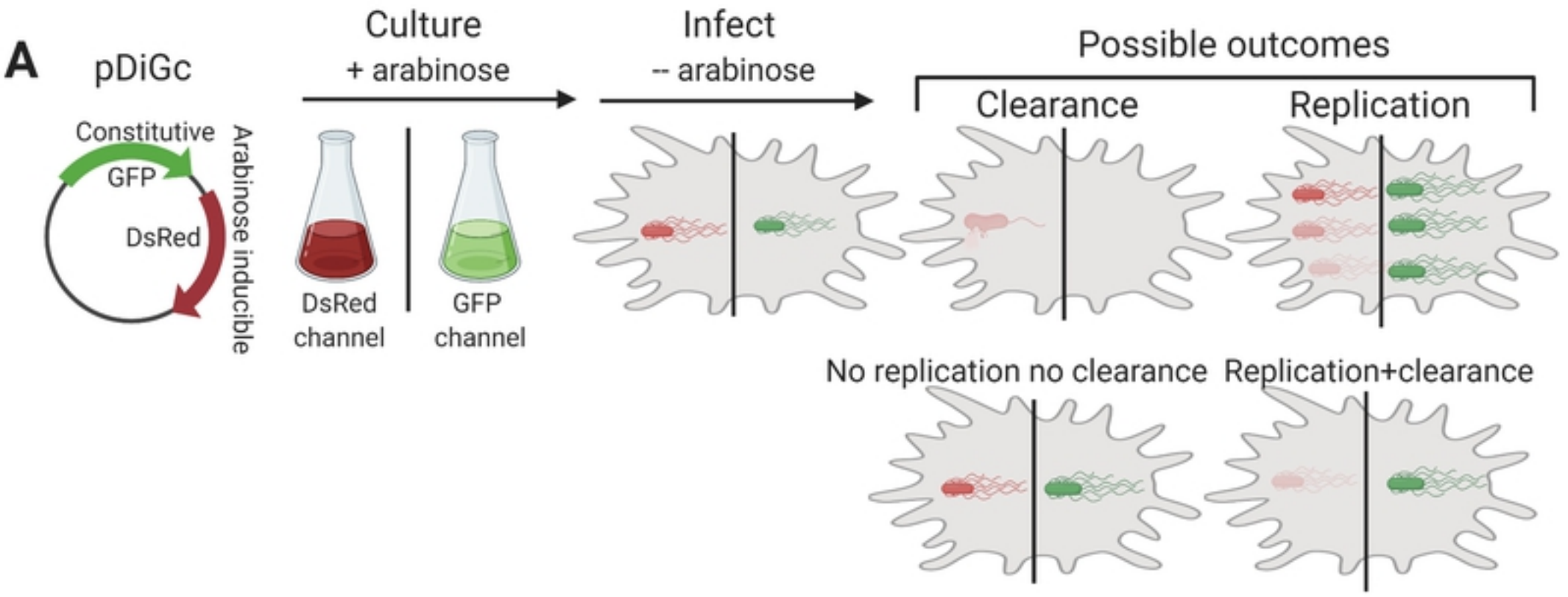

B

Media	[Zn] (μM)	[Y] (μM)	[Ga] (μM)	[Ca] (mM)	[Cu] (μM)	[Fe] (μM)	[Mn] (μM)
DMEM + 20% Chelex FBS	3.48	4.88	6.17	1.13	26.98	26.12	0.21
DMEM + 20% FBS	25.18	4.81	5.99	18.24	26.94	138.79	0.31

bioRxiv preprint doi: https://doi.org/10.1101/2021.03.18.436026; this version posted March 18, 2021. The copyright holder for this preprint (which was not certified by peer review) is the author/funder, who has granted bioRxiv a license to display the preprint in perpetuity. It is made available under aCC-BY 4.0 International license.

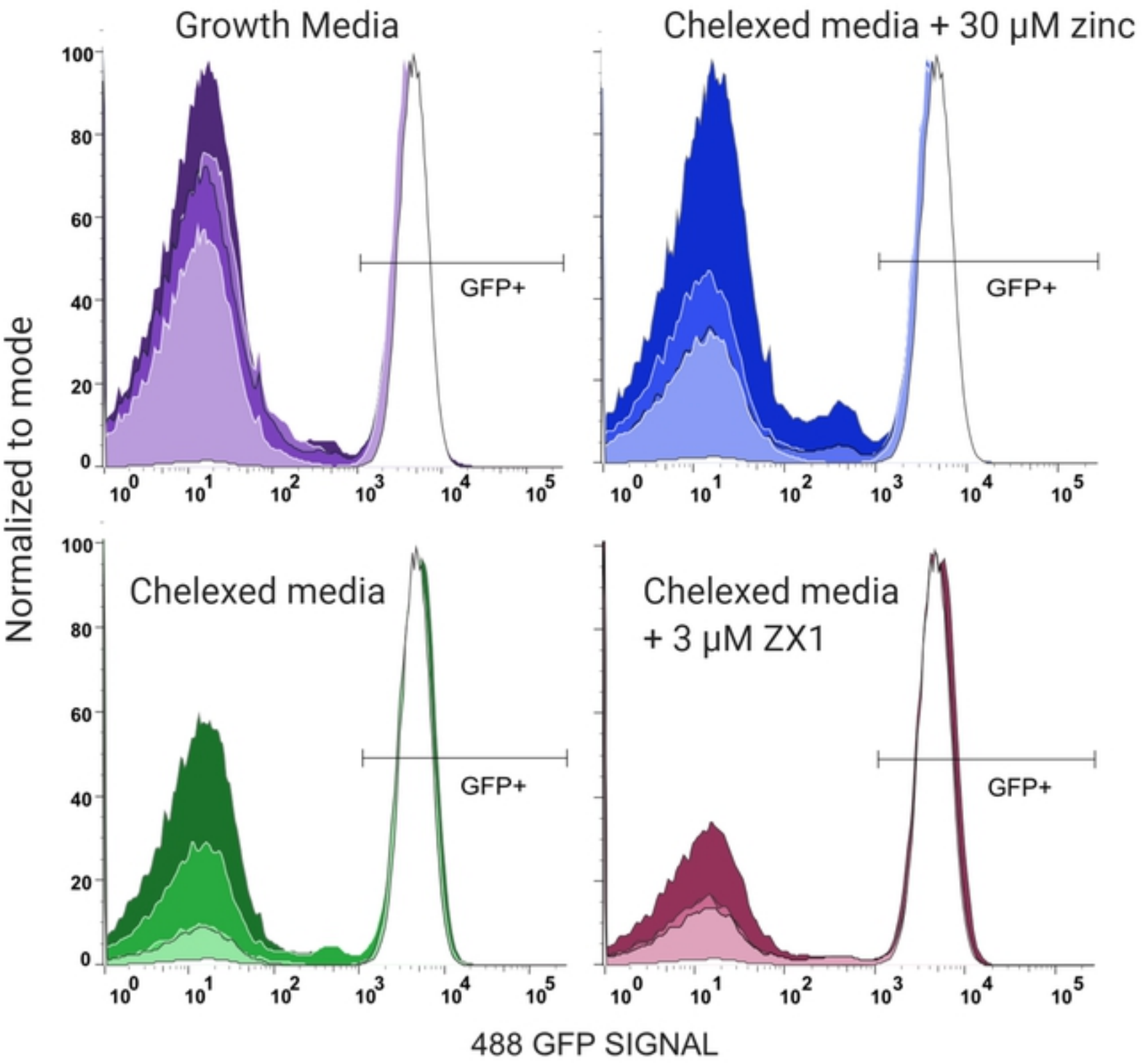

Figure 7

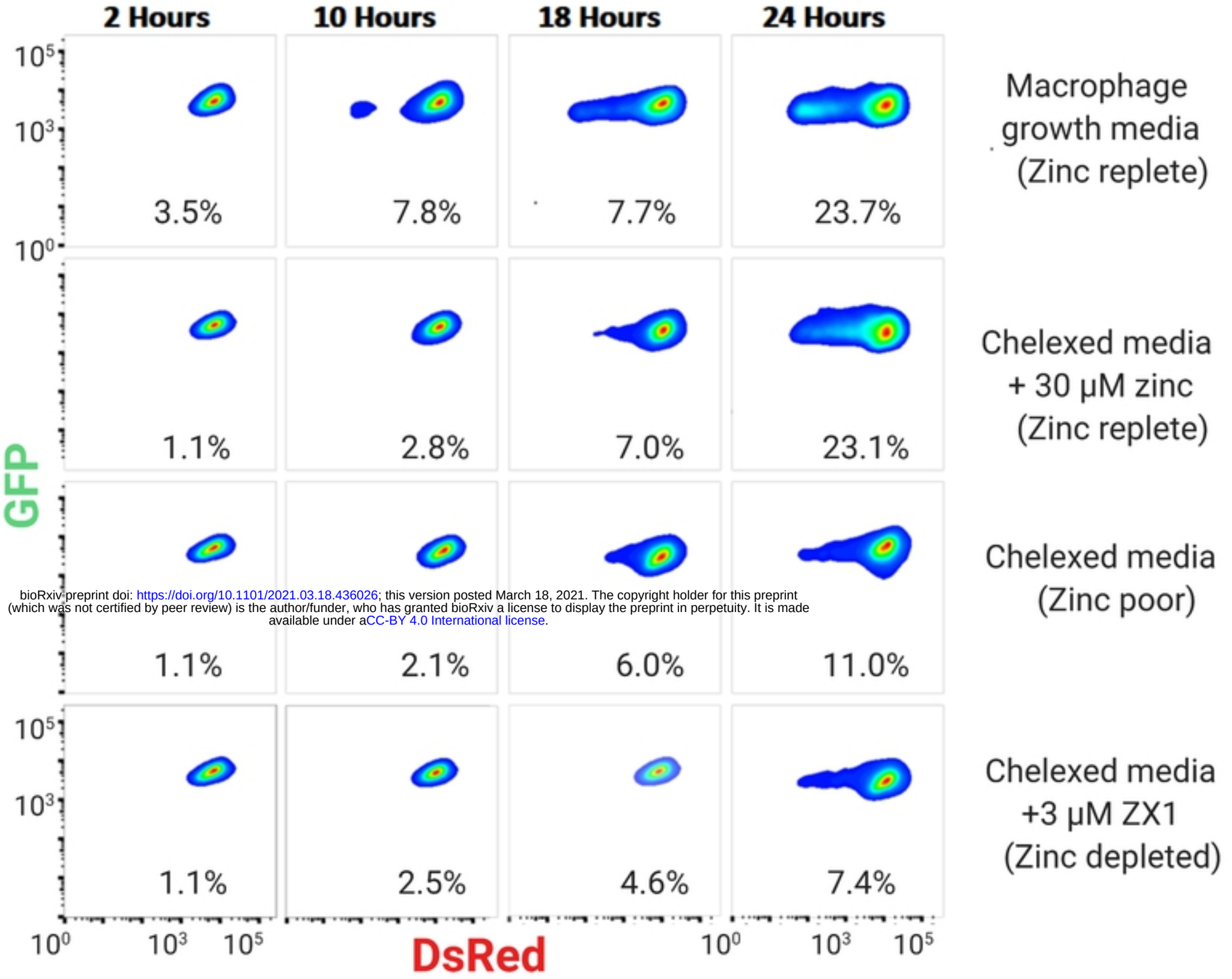

bioRxiv preprint doi: https://doi.org/10.1101/2021.03.18.436026; this version posted March 18, 2021. The copyright holder for this preprint (which was not certified by peer review) is the author/funder, who has granted bioRxiv a license to display the preprint in perpetuity. It is made available under aCC-BY 4.0 International license.

Figure 8

bioRxiv preprint doi: https://doi.org/10.1101/2021.03.18.436026; this version posted March 18, 2021. The copyright holder for this preprint (which was not certified by peer review) is the author/funder, who has granted bioRxiv a license to display the preprint in perpetuity. It is made available under aCC-BY 4.0 International license.

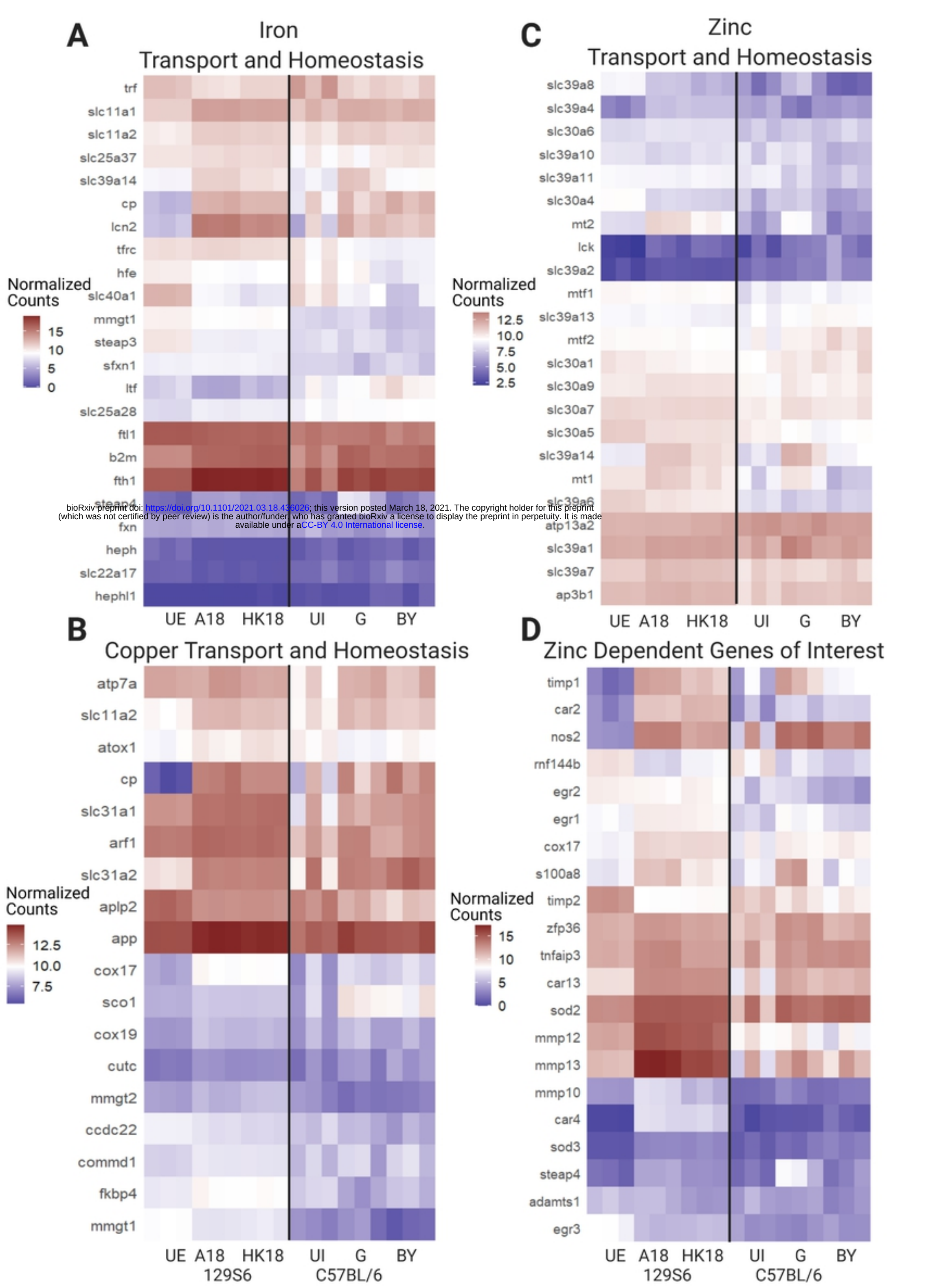

Figure 9